Local Climate Sensitivity: What Can Time Series of Distributions Reveal about Spatial Heterogeneity of Climate Change?*

J. Isaac Miller†

Abstract

Transient climate sensitivity relates total climate forcings from anthropogenic and other sources to surface temperature. Global transient climate sensitivity is well studied, as are the related concepts of equilibrium climate sensitivity and transient climate response, but spatially disaggregated local climate sensitivity is less so. An energy balance model and an easily implemented semiparametric statistical approach are proposed to estimate local climate sensitivity using the historical record and to assess its contribution to global transient climate sensitivity. Results suggest that areas dominated by ocean tend to import energy, they are relatively more sensitive to forcings, but they warm more slowly than areas dominated by land. Economic implications are discussed.

This Version: August 30, 2022

JEL Classification: C14, C23, Q54

Key words and phrases: transient climate sensitivity, local climate sensitivity, energy balance model, temperature anomalies, functional time series

*I appreciate insightful comments from Myles Allen, William A. (Buz) Brock, Yoosoon Chang, David Hendry, Joon Park, and participants of the 2016 Conference on Econometric Models of Climate Change (Aarhus), and the 2016 International Conference of Computational and Financial Econometrics (Seville), 2017 North American Summer Meeting of the Econometric Society (Washington University in St. Louis), the 2017 Midwest Econometrics Group Meeting (Texas A&M), and a colloquium at the University of Missouri. I am grateful to Kyungsik Nam, whose dissertation research provided some new insights into estimating the semiparametric cointegrating models in the paper. All errors are mine.

†Department of Economics, University of Missouri, 615 Locust Street, Columbia, Missouri 65211, USA, millerjisaac@missouri.edu.

1 Introduction

Attribution of the evident upward movement in global temperatures over recent decades is a topic of central importance in climate science and growing importance in economics. Characterizing and predicting the anthropogenic footprint on our climate is a difficult but important task, and one that has been tackled both by complex physical climate models and relatively simple statistical models that aim to make the most out of historical series by capturing their most salient properties. The latter are typically based on low-dimensional energy balance models (EBMs). Statistical climate models that are complex enough to capture salient features of the data and make meaningful predictions yet simple enough to allow sufficient replications to assess uncertainty are useful to economists in estimating damages and comparing policies.

In particular, zero-dimensional EBMs provide physical bases for many statistical analyses that relate total radiative forcings (TRF) to global mean temperature anomalies (GMTA). The physical link is described by Gregory and Forster (2008) and Schwartz (2012), *inter alia*. A key parameter in these models, often labeled $1/\lambda$ and measured in °C/(W/m), is referred to as *transient climate sensitivity* or simply *climate sensitivity* (Boer and Yu, 2003; Held *et al.*, 2010).

A number of authors have estimated climate sensitivity using statistical methods applied to zero-dimensional EBMs. Recent methods generally allow for one of two types of long-run co-movement: cointegrating or co-breaking series. Proponents of the former argue that both TRF and GMTA have a common stochastic trend, and they include Stern and Kaufmann (2000), Kaufmann and Stern (2002), Kaufmann *et al.* (2006a, 2006b, 2010, 2013), and Pretis (2020). Those of the latter argue that TRF and GMTA have deterministic trends that have experienced one or more contemporaneous breaks, and they include Estrada *et al.* (2013a,b) and Estrada and Perron (2014). A lack of consensus among these authors suggests the use of statistical methods that maintain some robustness to either type of trending behavior in the data.

Zero-dimensional EBMs predict the temperature of a theoretically isothermal (spatially homogeneous) planet. While GMTA provides a convenient measure of central tendency, it ignores the temperature anomaly distribution, and thus zero-dimensional EBMs cannot account for spatial heterogeneity. In contrast, one-dimensional EBMs (Budyko, 1969; Sellers, 1969) account for heterogeneity in temperature and net (horizontal) heat transport (NHT) across latitudes, while two-dimensional EBMs (Sellers, 1976, North *et al.*, 1983) additionally account for heterogeneity within latitudes.

In this paper, a non-gridded one-dimensional EBM is proposed for the purpose of es-

timating spatially disaggregated climate sensitivity or *local climate sensitivity* using the historical record.[1] This model takes into account the distribution of spatially disaggregated temperature anomalies – or their fast components in the spirit of Held *et al.* (2010). Considering this distribution simplifies the statistical analysis relative to a gridded model without sacrificing as much information about global heterogeneity as is lost to aggregation for a zero-dimensional EBM or even for a one-dimensional EBM based on latitude.

A novel but easily implemented semiparametric estimation procedure using functional time series is proposed to estimate spatially heterogeneous NHT as a nonlinear function of temperature anomalies and it contribution to climate sensitivity. Not surprisingly, homogeneity is rejected. An NHT function is estimated that is strikingly nonconstant and nonlinear in temperature anomalies, but we show that the nonlinearity is consistent with the linear Budyko-Sellers model. Over the globe, oceans tend to be net importers of energy, while continents tend to be net exporters.

Spatial heterogeneity of NHT implied by the nonlinearity is an important feature of more complicated climate models (Trenberth *et al.*, 2001, e.g.). The geographical distribution of the estimated local climate sensitivities is roughly comparable to that of the analogous parameter mapped by Boer and Yu (2003) using a completely different approach and data. The heterogeneity of local climate sensitivity is tied to polar amplification, and recent work by Francis and Vavrus (2012), Liu *et al.* (2012), Screen and Simmonds (2013), *inter alia* emphasize a link between polar amplification and severe weather at mid-latitudes. The IPCC's Fifth Assessment Report (IPCC, 2014) echoes this link with a prediction of increasingly likely heat waves and "extreme precipitation events" over mid-latitudes. Increasingly frequent and severe weather events, such as the active Atlantic hurricane season of 2020, the historic European heatwave of 2022, and the massive flooding in Pakistan in 2022, certainly have had negative economic impacts. Moreover, as Brock and Xepapadeas (2017) point out, ignoring local differences in NHT – as economic models based on zero-dimensional EBMs do – may systematically bias optimal mitigation policy.

Both the proposed methodology and the empirical application of that methodology to climate change firmly link the present research to that of Professor Joon Y. Park, in addition to that of his wife and frequent coauthor, Professor Yoosoon Chang, some of his former students, and even a recent "grandstudent" of theirs. The link between a single time series and a time series of distributions is directly related to Professor Park's work on functional time series and less directly to that on functional coefficients in published papers by Park

[1] Chapman *et al.* (2013) use *local* trends in conjunction with climate sensitivity to describe heterogeneous climate responses in °C. In this paper, the terminology applies to local variations in the parameter $1/\lambda$, but of course these also imply differing local trends.

and Hahn (1999), Park *et al.* (2010), Park and Qian (2012), Chang *et al.* (2014, 2016a, 2016b, 2016c, 2020), Nam (2018), and Miller and Nam (2020) in addition to a number of as-yet unpublished papers. The latter three squarely lie within a growing literature on the analysis of climate and climate change using econometric methods, loosely termed *climate econometrics*, around which special issues of Journal of Econometrics, Energy Economics, and other journals have recently been organized.

The rest of the paper is organized as follows. Section 2 describes the physical and statistical models considered in this research, and then Section 3 proposes a simple estimation procedure that is summarized in three steps. Section 4 presents the data employed with results of the estimation procedure and discussions of these results. Section 5 concludes. An appendix contains technical details on the approximation to the EBM that is empirically analyzed in the paper.

2 Physical and Statistical Models

The first law of thermodynamics equates absorbed energy Q, incoming energy net of ice and land albedo (reflection), with radiated energy E of the Earth in a steady state (Peixoto and Oort, 1992; Taylor, 2005, e.g.). Both Q and E are functions of the Earth's effective temperature, but are often expressed as functions $Q(\bar{\tau})$ and $E(\bar{\tau})$ of surface temperature, denoted here by $\bar{\tau}$ (Schwartz, 2012, e.g.).

Following Schwartz (2012), planetary net heat flux into the planet in a zero-dimensional EBM is given by $N(\bar{\tau}) = h + Q(\bar{\tau}) - E(\bar{\tau})$ with the introduction of an external spatially uniform forcing h (TRF) expressed in W/m^2. $Q(\bar{\tau}) - E(\bar{\tau})$ is typically assumed to be linear in $\bar{\tau}$ due to Budyko's (1969) linear representation of E and with a constant ice line for Q, so we let $Q(\bar{\tau}) - E(\bar{\tau}) = QS - A - \lambda\bar{\tau}$ following North and Cahalan (1981) with constants Q, S, and A but replacing $-B$ in their notation with $-\lambda$ to match the notation of Schwartz (2012) for the derivative of $Q(\bar{\tau}) - E(\bar{\tau})$ with respect to $\bar{\tau}$.

The planetary net heat flux becomes

$$N(\bar{\tau}) = h + QS - A - \lambda\bar{\tau} \tag{1}$$

under the linear specification. Noting that global temperature is an implicit function of TRF h, total differentiation of equation (1) yields

$$dN(\bar{\tau}) = dh - \lambda d\bar{\tau}, \tag{2}$$

which is the well-known energy balance equation (EBM) of Gregory and Forster (2008,

equation 1), Schwartz (2012, equation 5), *inter alia*.[2]

Solving for a change in the global temperature $d\bar{\tau}$ resulting from a change in TRF dh yields

$$\frac{d\bar{\tau}}{dh} = \frac{1}{\lambda}\left[1 - \frac{d}{dh}N(\bar{\tau})\right], \tag{3}$$

which is the *climate sensitivity* (Boer and Yu, 2003; Held *et al.*, 2010), and it equals $1/\lambda$ in the steady state in which $dN(\bar{\tau}) = 0$. When the system is out of equilibrium, the derivative $d\bar{\tau}/dh$ is referred to as the transient climate sensitivity (Schwartz, 2012). Allowing for measurement errors and idiosyncrasies, climate sensitivity may be estimated by regressing GMTA onto TRF over the historical record (Estrada *et al.*, 2013b), similarly to equation (12) below.

Often discussed in the literature are the related concepts of equilibrium climate sensitivity (ECS) and transient climate response (TCR) (Bindoff *et al.*, 2013, e.g.). Both are defined as temperature responses to a doubling in atmospheric concentration of CO_2 from pre-industrial levels and both may be calculated from the transient climate sensitivity, but ECS takes into account ocean heat uptake, while TCR does not. In particular, TCR is $h_{2\times}d\bar{\tau}/dh$ with $h_{2\times} = 3.71$ W/m^2, and ECS relates to climate sensitivity by a parameter governing the ocean's heat uptake (Schwartz, 2012). It is appropriate to think of climate sensitivity, as defined here, as a model parameter and TCR and ECS as model outputs based on that parameter.

The EBM in equation (2) is described as zero-dimensional in the sense that temperature is homogeneous over the globe. While such an assumption is obviously unrealistic in and of itself, it allows simple analyses to estimate aggregate global characteristics of the climate, such as climate sensitivity. Budyko (1969) and Sellers (1969) extend the zero-dimensional planetary EBM to a one-dimensional EBM that allows for horizontal (advective) heat transport in the direction from the Equator to the poles known as *polar amplification*. At a given latitude θ (in radians), a forced EBM is given by

$$X(\tau_\theta - \bar{\tau}, \theta) = h + QS(\theta) - A - \lambda\tau_\theta, \tag{4}$$

where $X(\tau_\theta - \bar{\tau}, \theta)$ is NHT (outgoing for positive values), a function of latitude and the deviation of surface temperature τ_θ (itself a function of latitude) from global mean temperature $\bar{\tau}$, and where $S(\theta)$ depends on location (see North and Cahalan, e.g.) and integrates globally to S defined above.

A variety of generalizations of the one-dimensional EBM in equation (4) have been

[2]These two sets of authors write $N(\bar{\tau})$ and h in levels, because the steady-state unforced planetary net heat flux is zero. For small changes $dN(\bar{\tau}) \approx \triangle N(\bar{\tau}) = N(\bar{\tau}) - 0$ and $dh \approx \triangle h = h - 0$.

proposed. Two-dimensional EBMs allow heterogeneity in temperature based on other geographic characteristics, such as land vs. ocean coverage (Sellers, 1976; North *et al.*, 1983, e.g.). Moist EBMs such as that of Langen and Alexeev (2007) and Merlis and Henry (2018) allow for water vapor in the atmosphere, while Siler *et al.* (2018) take moist EBMs a step further by allowing for the effect of the Hadley Circulation in the tropics.

These approaches rely on an EBM defined over a continuum of temperatures that are themselves defined over a continuum of latitudes. Simple "two-box" models such as that of Langen and Alexeev (2007) can be derived from underlying continuous processes and aggregate concepts such as the global mean are derived accordingly. However, statistical estimation of local climate sensitivity requires spatially disaggregated data, so discretization to a much finer resolution than that of a two-box model or a global aggregate is needed. We define functions of spatially disaggregated data, such as the global mean temperature $\bar{\tau}$, as aggregates of observations τ_L drawn systematically from locations $L(\theta, \varphi)$ given by grid boxes of equal latitude θ and equal longitude φ.

To ameliorate measurement errors acknowledged in the climate literature, disaggregated temperature data typically are expressed as temperature anomalies $r_L = \tau_L - \tau_L^B$, where τ_L^B is the mean temperature over box L during a base period. The expression

$$X(r_L, L) = h + QS(L) - A - \lambda(r_L + \tau_L^B) \tag{5}$$

gives a two-dimensional EBM that is a function of discrete boxes L, but that is derived in the appendix as discretization of a two-dimensional EBM that is continuous in latitude and longitude.

We further define the NHT function $X(r)$ to be a locationless measure of NHT at temperature anomaly r, which is calculated as the average NHT $X(r_L, L)$ over all boxes $\{L : r_L = r\}$ that have the same temperature anomaly r at a given time. The EBM can be written as

$$X(r) = h + QS(r) - A - \lambda(r + \tau^B(r)), \tag{6}$$

where τ^B is defined to be the average of the base temperatures over the set of locations $\{L : r_L = r\}$ and is thus a nonlinear function of r and $S(r)$ is defined analogously to $X(r)$. See the appendix for further details. Note that the nonlinearity in r allows for spatial heterogeneity of NHT.

It is useful to step back and consider the significance of r and $X(r)$ more carefully. Aggregating NHT across locations using $X(r)$ groups them by anomaly. In order for sharp distinctions between NHT at different locations to remain, those locations must share common characteristics. Such commonality is certainly plausible in the North Atlantic, in the

Arctic, and around Greenland, where some of the largest anomalies occur, or in the Tropics, where some of the smallest occur. The aggregation reduces the model to a single dimension r, like that of early one-dimensional EBMs. However, NHT is not a function of latitude as it is in those models, allowing for more realistic complexity. For examples, the Southern Ocean has not warmed as fast as the Arctic Ocean, as a one-dimensional EBM implies it should.

As a frame of reference, Leduc *et al.* (2016) aggregate temperatures by region in order to assess temperature change as a function of cumulative carbon emissions. They find the relationship to be strikingly linear in most regions (see their Figure 2), supportive of the linearity of regional NHT functions along the lines of Budyko-Sellers EBM discussed above. Yet, their slopes are quite different across regions, supporting the nonlinearity of $X(r)$ to capture spatial heterogeneous climate sensitivity. Indeed, nonlinearity of $X(r)$ induced by aggregation may explain why the evidence for linearity in some of the regions considered by Leduc *et al.* (2016) is stronger than in others. Regions with relatively homogeneous NHT – near the Equator, say – have nearly linear NHT functions, and the results of those authors are consistent with this reasoning.

The work of Castruccio *et al.* (2014) provides another frame of reference, both due to the long-run linearity of temperature in forcings imposed by those authors (as derived by Miller and Brock, 2021) in emulating model output and the comparison in their Figure 6 with pattern scaling. Pattern scaling assumes a linear relationship between local anomalies and GMTA. If the relationship between GMTA and TRF is also linear, pattern scaling imposes linearity of local NHT. The logic of nonlinearity resulting from aggregating heterogeneous climate sensitivities discussed above is therefore not inconsistent with linearity assumption of pattern scaling.

A methodological benefit of the aggregation across anomalies is that $X(r)$ may be viewed as a functional in a Hilbert space. Specifically, we define the Hilbert space H similarly to Chang *et al.* (2016c, 2020) but without temporal demeaning, as

$$H = \left\{ w \left| \int w^2(r) dr < \infty \right. \right\}, \tag{7}$$

with inner product $\langle v, w \rangle = \int v(r) w(r) dr$ for $v, w \in H$, where the integrals are evaluated over the range of temperature anomalies $[r^-, r^+]$.

The distribution of temperature anomalies, given by $f(r)$, is a functional in that space that has been employed already by Chang *et al.* (2020) and Miller and Nam (2020). The former analyzed and tested for the type of nonstationarity in the temporal evolution of the temperature anomaly distribution, while the latter used the distribution of ocean tempera-

ture anomalies to measure a multidecadal and multibasin temperature cycle to predict the next slowdown in global warming.

Integrating the EBM in equation (6) over all temperature anomalies observed at a given time yields

$$\langle X, f\rangle = h + QS - A - \lambda\bar{\tau}, \tag{8}$$

where $S = \langle S, f\rangle$ and $\bar{\tau} = \langle \tau, f\rangle$ are the same as in equation (1) up to an approximation error.[3] The right hand sides of equations (1) and (8) are the same, but the left-hand sides appear to be different. In fact, the left-hand sides of both equations are zero. The left-hand side of equation (1) shows planetary incoming energy less aggregate outgoing planetary energy, which must be zero in equilibrium. In contrast, the left-hand side of equation (8) shows aggregate net energy transported horizontally from each region of the globe, which must also aggregate to zero. Even when the planet is in a state of equilibrium, so that $N(\bar{\tau}) = 0$, $X(r)$ will be positive over some regions (energy "exporters") and negative over others (energy "importers").

How does the EBM in equation (8) change when the climate is forced? Going back to equations (2) and (3) for the globe, a change in forcing drives a change in GMTA, which is reflected by $1/\lambda$ when planetary net heat flux is zero. In order for that to happen, f must be an implicit function of h. We maintain the assumption discussed above that $Q(\bar{\tau}) - E(\bar{\tau})$ is linear in temperature $\bar{\tau}$ globally, and we extend it to apply locally. In particular, we assume that local changes in the temperature anomaly distribution affect the local temperature but not $S(\theta)$.

Analogously to equations (2) and (3), we differentiate equation (8) to get

$$d\langle X, f\rangle = dh - \lambda d\bar{\tau}, \tag{9}$$

and

$$\frac{d\bar{\tau}}{dh} = \frac{1}{\lambda}\left[1 - \frac{d}{dh}\langle X, f\rangle\right] = \frac{1}{\lambda}\left[1 - \left\langle X, \frac{df}{dh}\right\rangle\right], \tag{10}$$

where the last equality follows by assuming that the NHT function $X(r)$ is invariant with respect to TRF.[4]

The conclusion that $d\bar{\tau}/dh = 1/\lambda$ in the steady state holds for both equations (3) and (10). Although planetary net flux must be zero in a steady state equilibrium, local

[3]The approximation error comes from weighting all grid boxes equally to obtain equation (8) as discussed in the Appendix. The plots labeled *HadCRUT5 Mean Anomalies* and *Estimated Mean Anomalies* in Figure 1 show estimates of GMTA using equal weights to be very similar to those weighted by latitude.

[4]Empirical evidence not shown allowing for time-variation in the estimation scheme discussed below suggests that $dX/dh \approx 0$ for all r, so this assumption seems reasonable.

NHT might never be zero, because the temperature anomaly distribution may change. Casual observation of the data suggest that this distribution does in fact change over time, and Chang *et al.* (2020) provide evidence supporting an even stronger result that the distributions are stochastically trending over time. Clearly $df/dh \neq 0$.

In order to express heterogeneous NHT more explicitly, equation (10) may be rewritten as

$$\frac{d\bar{\tau}}{dh} = \langle 1, C \rangle / (r^+ - r^-)$$

where

$$C(r) = \frac{1}{\lambda}\left(1 - X(r)\frac{df(r)}{dh}(r^+ - r^-)\right) \tag{11}$$

is defined to be the *local climate sensitivity* (LCS, henceforth), expressed in $°\text{C}/(\text{W}/\text{m}^2)$. NHT across the globe integrates to zero, so that climate sensitivity, given by the normalized integral of local climate sensitivities across all temperature anomalies, is $d\bar{\tau}/dh = 1/\lambda$ just as with the zero-dimensional EBM used to obtain equation (3).

The negative sign after $1/\lambda$ in $C(r)$ implies that as TRF increases, areas that pass along the additional energy from this increase by exporting it ($X(r) > 0$) are less sensitive to changes in TRF ($C(r) < 1/\lambda$). Those that do not pass along the additional energy and thus import energy on net ($X(r) < 0$) are more sensitive to changes in TRF ($C(r) > 1/\lambda$).

3 Methodology

3.1 Estimation of LCS

We propose estimating the LCS by separately estimating each component of $C(r)$ in equation (11): $df(r)/dh$, $1/\lambda$, and $X(r)$. $f(r)$ is estimated over each year $t = 1, ..., T$, and $f(r)$, $df(r)/dh$, and $X(r)$ are estimated at equidistant points $r_i \in [r^-, r^+]$ for $i = 0, 1, ..., n$, such that $r_0 = r^-$, $r_n = r^+$, $\epsilon = r_i - r_{i-1}$, and thus $(r^+ - r^-) = n\epsilon$ for some small number ϵ, which we set to be 0.005.

3.1.1 Step 1: $df(r)/dh$.

Before estimating $df(r)/dh$, the density $f_t(r)$ is for each year t using a standard kernel density estimator. Because global temperature anomaly data sets contain a large number of cross-sectional (spatial) observations for each time period, estimates of $f_t(r)$ are precise enough that we make no further distinction between the densities and their estimates, following Chang *et al.* (2020) and Miller and Nam (2020).

One way to estimate $df(r)/dh$ is by linear regression. Specifically, this task is accomplished by regressing $f_t(r_i)$ at each r_i on h_t and an intercept. Estimates of the coefficient on h_t from these $n-1$ regressions estimate the derivative $df(r_i)/dh$ at each r_i.

3.1.2 Step 2: Climate Sensitivity, $1/\lambda$.

Because the last term of equation (10) equals zero, climate sensitivity is given by the first term, $1/\lambda$. Estimating $1/\lambda$ is straightforward using linear regression. To this end, a conditional expectation function may be defined as

$$\langle \iota, f_t \rangle = \mathbf{E}[\langle \iota, f_t \rangle | h_t] + \langle \varepsilon_{S0}, f_t \rangle ,$$

where $\langle \iota, f_t \rangle$ with identity function $\iota(r)$ is the GMTA and $\langle \varepsilon_{S0}, f_t \rangle = \langle \iota, f_t \rangle - \mathbf{E}[\langle \iota, f_t \rangle | h_t]$ may be interpreted as the aggregate of errors resulting from stochastic forcing (North *et al.*, 1981), measurement error, or other sources of ephemeral disequilibrium.

Adding and subtracting $\alpha_{S0,0} + \alpha_{S0,1} h_t$ yields

$$\langle \iota, f_t \rangle = \alpha_{S0,0} + \alpha_{S0,1} h_t + (\mathbf{E}[\langle \iota, f_t \rangle | h_t] - (\alpha_{S0,0} + \alpha_{S0,1} h_t)) + \langle \varepsilon_{S0}, f_t \rangle ,$$

where the third term reflects unmodeled nonlinearity in the spatial aggregate. In fact, we know that $d\bar{r}/dh = d\bar{\tau}/dh$ is constant in the physical model, so the third term reduces to zero. By defining $\varepsilon_{S0t} = \langle \varepsilon_{S0}, f_t \rangle$ the model may be written simply as

$$S0 : \bar{r}_t = \alpha_{S0,0} + \alpha_{S0,1} h_t + \varepsilon_{S0t}, \tag{12}$$

for $t = 1, ..., T$ years. We may interpret $\alpha_{S0,1}$ as the climate sensitivity, or more precisely as global mean climate sensitivity, given by $1/\lambda$, as long as the unmeasured forcing ε_{S0t} is idiosyncratic with respect to changes in the measured forcing h_t.

The simple linear regression in equation (12) is employed by Estrada *et al.* (2013b) and other authors to estimate climate sensitivity. Those authors explicitly link the regression model to a zero-dimensional EBM, but we have now shown how it also links to a higher-dimensional EBM.

3.1.3 Step 3: NHT Function, $X(r)$.

The most complicated task and main methodological contribution of this research is to estimate the local NHT function $X(r)$. As a simple motivating example, suppose we know that $X(r)$ is quadratic such that $X(r)/\lambda = \gamma_0 + \gamma_1 r + \gamma_2 r^2$ with unknown γ_0, γ_1, and γ_2. The regression given by Model $S0$ in equation (12) is motivated by equation (10) with

the equilibrium condition that $\langle X, df \rangle = 0$. But if the equilibrium condition holds only in expectation then information about the NHT function may be gleaned from adjustment to that equilibrium, which motivates including the NHT function directly into the regression.

Substituting the equilibrium condition

$$\mathbf{E}\langle X/\lambda, f_t \rangle = \mathbf{E}\left\langle \gamma_0 + \gamma_1 \iota + \gamma_2 \iota^2, f_t \right\rangle = 0 \tag{13}$$

into Model $S0$ and recalling that $\langle \iota, f_t \rangle = \bar{r}_t$ and $\langle 1, f_t \rangle = 1$ for all t yields

$$\bar{r}_t = \alpha_{S0,0} + \alpha_{S0,1} h_t + (\gamma_0 + \gamma_1 \bar{r}_t + \gamma_2 \left\langle \iota^2, f_t \right\rangle) + \tilde{\varepsilon}_{S0t}, \tag{14}$$

where $\tilde{\varepsilon}_{S0t} = \varepsilon_{S0t} + (\mathbf{E}\langle X/\lambda, f_t \rangle - \langle X/\lambda, f_t \rangle)$. The parameter γ_0 is not identified due to the presence of $\alpha_{S0,0}$. The parameter γ_1 is not identified either, because $\bar{r}_t$ appears on both sides of the equation. For known parameters γ_0 and γ_1, equation (14) becomes a feasible regression and γ_2 is identified.

We condition out the nuisance terms γ_0 and $\gamma_1 \bar{r}_t$ to estimate γ_2. Define δ_{20} and δ_{21} by

$$\begin{bmatrix} \delta_{20} \\ \delta_{21} \end{bmatrix} = \left(\mathbf{E} \begin{bmatrix} 1 \\ \bar{r}_t \end{bmatrix} \begin{bmatrix} 1 \\ \bar{r}_t \end{bmatrix}' \right)^{-1} \mathbf{E} \begin{bmatrix} 1 \\ \bar{r}_t \end{bmatrix} \left\langle \iota^2, f_t \right\rangle$$

so that $x_{2t} = \left\langle \iota^2, f_t \right\rangle - \delta_{21} \bar{r}_t - \delta_{20}$ orthogonalizes $\left\langle \iota^2, f_t \right\rangle$ and the quadratic in parentheses in equation (14) more generally with respect to GMTA and a constant. Specifically, x_{2t} is estimated by the series of fitted residuals from a regression of $\left\langle \iota^2, f_t \right\rangle$ onto $\bar{r}_t$ and a constant with linear projection coefficients given by δ_{21} and δ_{20}.

The orthogonalization allows a feasible regression given by

$$S1 : \bar{r}_t = \alpha_{S0,0} + \alpha_{S0,1} h_t + x_{2t} \gamma_2 + \tilde{\varepsilon}_{S0t} \tag{15}$$

in place of the infeasible regression in equation (14). Co-movements of the components of the equilibrium condition in equation (13) with the GMTA $\bar{r}_t$ are removed, leaving only adjustments to the equilibrium given by non-zero γ_2.

Having estimated δ_{20} and δ_{21} using the regression to obtain x_{2t} and having estimated γ_2 using the regression in equation (15), we can now identify γ_0 and γ_1. Setting

$$x_{2t}\gamma_2 = \gamma_2(\left\langle \iota^2, f_t \right\rangle - \delta_{21}\bar{r}_t - \delta_{20}) = (\gamma_0 + \gamma_1 \bar{r}_t + \gamma_2 \left\langle \iota^2, f_t \right\rangle)$$

equates the models in equations (14) and (15). We could identify $\gamma_0 = -\gamma_2 \delta_{20}$ and $\gamma_1 = -\gamma_2 \delta_{21}$ in this way.

Suppose we want to impose the stronger equilibrium condition that $\langle X, f\rangle = 0$ and not only in expectation. Setting $\gamma_0 = \gamma_1 = \gamma_2 = 0$ trivially accomplishes this task. With a non-zero γ_2, however, the same condition is imposed by introducing a time-varying intercept identified by

$$\gamma_{0t} = -\gamma_1 \bar{r}_t - \gamma_2 \left\langle \iota^2, f_t \right\rangle = -\gamma_2(\left\langle \iota^2, f_t \right\rangle - \delta_{21} \langle \iota, f_t \rangle)$$

so that $x_{2t} = 0$. This gives us an alternative to identify γ_0 while at the same time allowing for a time-varying NHT.

Results not shown show very little change in the intercept over time, so that

$$-\gamma_2\delta_{20} \approx -\gamma_2(\left\langle \iota^2, f_t \right\rangle - \delta_{21} \langle \iota, f_t \rangle) \approx -\gamma_2(\left\langle \iota^2, f \right\rangle - \delta_{21} \langle \iota, f \rangle)$$

with f defined as an average of (f_t) over time for each r_i in its support. The first approximation would be an equality under the stricter equilibrium condition that $x_{2t} = 0$ and the last approximation follows from the empirical finding that the relationship is stable over time, so we identify γ_0 as $-\gamma_2(\left\langle \iota^2, f \right\rangle - \delta_{21} \langle \iota, f \rangle)$.

In fact, a time-invariant relationship is consistent with the literature. Estrada *et al.* (2013b) allow for structural instability (breaks) in the trends of TRF and GMTA, yet they find that the series break together so that their relationship is stable. Eroğlu *et al.* (2022) explicitly test for time-varying cointegration against linear cointegration, and find that GMTA linearly cointegrates with well-mixed greenhouse gases, the most persistent component of TRF.

Finally, in the case of a known quadratic, $X(r)$ is identified by dividing $\gamma_0 + \gamma_1 r + \gamma_2 r^2$ by the climate sensitivity $1/\lambda$, an estimate of which comes from the estimate of $\alpha_{S0,1}$ in Model $S0$ in equation (12). This completes the estimation procedure for a known quadratic NHT function.

More generally, assume that the NHT function admits a series expansion that is approximated by

$$X/\lambda = \gamma_0 + \gamma_1 r + \gamma'_{2:m} g_{2:m}(r)$$

with known functions $g_{2:m}(r) = (g_2(r), ..., g_m(r))'$ and $\gamma_{2:m} = (\gamma_2, ..., \gamma_m)'$ for $m \geq 2$. This assumption is in the spirit of the assumption of North (1975) that the NHT function admits a Legendre polynomial expansion in latitude, except that we have aggregated over locations with common observed anomalies.

The logic of the infeasibility of equation (14) remains. Rather than a single regression to create a series of fitted residuals x_{2t} as above, orthogonalization is accomplished using

$m-1$ regressions given by

$$\begin{aligned}
\bar{g}_{2t} &= \delta_{20} + \delta_{21}\bar{r}_t + x_{2t} \\
\bar{g}_{3t} &= \delta_{30} + \delta_{31}\bar{r}_t + \delta_{32}\bar{g}_{2t} + x_{3t} \\
&\vdots \\
\bar{g}_{mt} &= \delta_{m0} + \delta_{m1}\bar{r}_t + \delta_{m2}\bar{g}_{2t} + \cdots + \delta_{m,m-1}\bar{g}_{m-1,t} + x_{mt}.
\end{aligned} \tag{16}$$

with $\bar{g}_{it} = \langle g_i, f_t \rangle$ for $i = 2, ..., m$,

$$\begin{bmatrix} \delta_{20} \\ \delta_{21} \end{bmatrix} = \left(\mathbf{E} \begin{bmatrix} 1 \\ \bar{r}_t \end{bmatrix} \begin{bmatrix} 1 \\ \bar{r}_t \end{bmatrix}' \right)^{-1} \mathbf{E} \begin{bmatrix} 1 \\ \bar{r}_t \end{bmatrix} \bar{g}_{2t}$$

analogously to δ_{20} and δ_{21} defined above, and

$$\begin{bmatrix} \delta_{i0} \\ \delta_{i1} \\ \delta_{i2} \\ \vdots \\ \delta_{i,i-1} \end{bmatrix} = \left(\mathbf{E} \begin{bmatrix} 1 \\ \bar{r}_t \\ \bar{g}_{2t} \\ \vdots \\ \bar{g}_{i-1,t} \end{bmatrix} \begin{bmatrix} 1 \\ \bar{r}_t \\ \bar{g}_{2t} \\ \vdots \\ \bar{g}_{i-1,t} \end{bmatrix}' \right)^{-1} \mathbf{E} \begin{bmatrix} 1 \\ \bar{r}_t \\ \bar{g}_{2t} \\ \vdots \\ \bar{g}_{i-1,t} \end{bmatrix} \bar{g}_{it}$$

for $i = 3, ..., m$.

The system in equation (16) may be rewritten more succinctly as

$$x_{2:m,t} = \Delta \langle g_{2:m}, f_t \rangle - \delta_1 \bar{r}_t - \delta_0 \tag{17}$$

by defining $x_{2:m,t} = (x_{2t}, ..., x_{mt})'$, an $(m-1) \times (m-1)$ matrix given by

$$\Delta = \begin{bmatrix} 1 & 0 & \cdots & 0 \\ -\delta_{32} & \ddots & \ddots & \vdots \\ \vdots & \ddots & \ddots & 0 \\ -\delta_{m2} & \cdots & -\delta_{m,m-1} & 1 \end{bmatrix},$$

and $(m-1) \times 1$ vectors given by $\delta_k = (\delta_{2k}, ..., \delta_{mk})'$ for $k = 0, 1$.

Model $S0$ is augmented as Model $S1$, generalized from that of equation (15) in the quadratic case to

$$S1 : \bar{r}_t = \alpha_{S1,0} + \alpha_{S1,1} h_t + x'_{2:m,t}\beta + \varepsilon_{S1t}, \tag{18}$$

such that $\gamma'_{2:m} = \beta'\Delta$. Model $S1$ is a semiparametric regression where $x_{2:m,t}$ represents the fitted residuals from the regressions in (16) and implied by (17). Parameters $\alpha_{S1,0}$, $\alpha_{S1,1}$, and β may be estimated using least squares.

The final step to obtain X/λ is to identify the γ's. Analogously to the simpler quadratic example, this is accomplished by setting $\gamma_1 = -\beta'\delta_1$ and $\gamma'_{2:m} = \beta'\Delta$, and the intercept is identified as $\gamma_0 = -\gamma_1 \langle \iota, f \rangle - \gamma'_{2:m} \langle g_{2:m}, f \rangle$, but δ_0 is not used in identification. Once again $X(r)$ is obtained by dividing the resulting function $\gamma_0 + \gamma_1 r + \gamma'_{2:m} g_{2:m}(r)$ by the climate sensitivity $1/\lambda = \alpha_{S0,1}$ estimated by Model $S0$ in the previous step.

3.1.4 Synthesis: Local Climate Sensitivity, $C(r)$.

A brief summary of the three steps for estimation follows.

1. Estimate $f_t(r)$ using a standard density estimation technique, then estimate $df(r)/dh$ by regressing $f_t(r_i)$ onto h_t and an intercept at points $r_i \in [r^-, r^+]$. Retain the estimates of the coefficients on h_t as $df(r_i)/dh$.

2. Estimate $1/\lambda$ by regressing $\bar{r}_t$ onto h_t and an intercept, as in Model $S0$ in equation (12). Retain the estimate of the coefficient $\alpha_{S0,1}$ on h_t.

3. Estimate $X(r)$.

   (a) Iteratively regress $\langle g_i, f_t \rangle$ onto an intercept, $\langle g_j, f_t \rangle$ for all $j < i$, and $\bar{r}_t$, as in equation (17). Retain the estimates of δ_1, Δ, and $(x_{2:m,t})$.

   (b) Estimate β using Model $S1$ in equation (18) by regression.

   (c) Identify $\gamma_1 = -\beta'\delta_1$, $\gamma'_{2:m} = \beta'\Delta$, and $\gamma_0 = -\gamma_1 \langle \iota, f \rangle - \gamma'_{2:m} \langle g_{2:m}, f \rangle$ with f defined as an average of (f_t) over time.

   (d) Set $X(r) = (\gamma_0 + \gamma_1 r + \gamma'_{2:m} g_{2:m}(r))/\alpha_{S0,1}$.

These steps require techniques no more complicated than kernel density estimation and least squares. Once the three components have been estimated, $C(r)$ is assembled from equation (11). Specifically, $C(r_i) = \alpha_{S0,1} - \alpha_{S0,1} X(r_i)(df(r_i)/dh)\epsilon$ gives the local climate sensitivity near each of n points r_i.

3.2 Time Scales and Dynamic Statistical Models

The discussion thus far has focused on static statistical models. In fact, there are equilibria occurring in two time scales in the static model. Planetary net heat flux is zero on a

multidecadal time scale (long-run, in the statistical model), but NHT integrates to zero on a subannual time scale (instantaneous, in the statistical model).

Held *et al.* (2010) and the IPCC's Fifth Assessment Report (Chapter 10, Bindoff *et al.*, 2013) differentiate two (additional) time scales in the context of a two-compartment zero-dimensional EBM. Specifically, they identify "fast" and "recalcitrant" components of temperatures. The fast component is proportional to forcings and, based on simulations of a general circulation model, they find that it reverts from 2.5°C to zero about one decade after an abrupt return of TRF to pre-industrial levels. A first-order autoregressive model is appropriate for a 10-year rate of decay.

To take into account the additional time scales, the static Model $S0$ is replaced by a dynamic model, Model $D0$, given by

$$D0 : \bar{r}_t^F = \rho_{D0}\bar{r}_{t-1}^F + \alpha_{D0,0} + \alpha_{D0,1}h_t + \varepsilon_{D0t}, \tag{19}$$

where $\bar{r}_t^F = \bar{r}_t - d_t$ is the fast component of GMTA and d_t is the recalcitrant component. The additional term $\rho_{D0}\bar{r}_{t-1}^F = \rho_{D0}\left\langle \iota, f_{t-1}^F \right\rangle = \rho_{D0}(\langle \iota, f_{t-1} \rangle - d_{t-1}) = \rho_{D0}(\bar{r}_{t-1} - d_{t-1})$ captures prior forcings still relevant to the present fast component.

The coefficient $\alpha_{D0,1}$ gives the immediate response of the fast component to a unit change in TRF. If $d_t = 0$ for all t, there is no recalcitrant component and the long-run (multidecadal) climate sensitivity is estimated by $\alpha_{D0,1}/(1-\rho_{D0}) \approx \alpha_{S0,1}$. More realistically, some of the upward movement in temperatures that would have been attributed to an increasing TRF will instead be accounted for by an increasing recalcitrant component, so that $\alpha_{D0,1}/(1-\rho_{D0}) < \alpha_{S0,1}$. In other words, the recalcitrant component tempers the climate sensitivity apparent in the historical record.

A dynamic model given by

$$D1 : \bar{r}_t^F = \rho_{D1}\bar{r}_{t-1}^F + \alpha_{D1,0} + \alpha_{D1,1}h_t + x'_{2:m,t}\beta + \varepsilon_{D1t}, \tag{20}$$

is analogous to Model $S1$. In Model $D1$, $x_{2:m,t}$ is redefined as

$$x_{2:m,t} = \Delta\left\langle g_{2:m}, f_t^F \right\rangle - \delta_1\bar{r}_t^F - \delta_0 - \delta_{-1}\bar{r}_{t-1}^F \tag{21}$$

so that the residuals are also orthogonal to the autoregressive term in Model $D1$. The parameters β, Δ, etc., are redefined accordingly. The parameters γ_0, γ_1, and $\gamma_{2:m}$ are identified in exactly the same way as with the static model with using β, Δ, and δ_1 but using neither δ_0 nor δ_{-1}.

4 Data and Empirical Results

4.1 Data Sources and Construction

HadCRUT5 temperature anomaly data[5] from Morice *et al.* (2020) are employed to measure temperature anomalies. Monthly HadCRUT5 data observed over 5° latitude by 5° longitude grid boxes are pooled into years over the time period 1850-2018 ($T = 169$), providing up to $36 \times 72 \times 12 = 31,104$ data points per year for the globe. The base period for the HadCRUT5 anomaly data is 1961-1990.

Annual global data[6] from Hansen *et al.* (2017) are used to proxy for spatially uniform TRF. Specifically, TRF is given by the sum of all but volcanic forcings following Estrada *et al.* (2013b). It is not hard to find deficiencies in the proxy: the effect of aerosols is notoriously difficult to pin down and most of the forcings are far from being spatially uniform.

An alternative would be to use only well-mixed greenhouse gases, which are nearly uniform by virtue of being well-mixed and are measured most precisely. Because there seems to be a consensus in the literature that both temperatures and forcings have a nonstationary (stochastic or deterministic) trend as discussed above, short-lived measurement error should not bias estimation. In this light, including series with short-lived measurement error may be preferable to omitting those series.

Six models are initially compared. The two static models and two dynamic models given by Model $S0$, $S1$, $D0$, and $D1$ are included. Further, S^+0 and D^-0 are included as comparisons with $S0$ and $D0$. They are analogous to $S0$ and $D0$, but with an accounting of the recalcitrant component d_t added to $S0$ and removed from $D0$.

Held *et al.* (2010) estimate the recalcitrant component of temperature by taking the average of simulated temperatures 10-30 years after an abrupt shutoff of TRF in their general circulation model at years 2000 and 2100 under the projection that CO_2 increases to 720 ppm by 2100. Doing so estimates the pre-industrial recalcitrant component (0°C), that in 2000 (0.1°C), and that in 2100 (0.4°C) under their projection. In the present analysis, the recalcitrant component d_t is calculated as piecewise linear, passing through the two anomalies above in 2000 and 2100 and through 0°C in 1880, and then demeaned by the average of the piecewise linear function over the HadCRUT5 base period of 1961-1990, (0.08°C) so that the recalcitrant component of the anomalies crosses zero between 1975 and 1976.

[5]Ensemble mean of HadCRUT5.0.0.0 downloaded from `https://www.metoffice.gov.uk/hadobs/hadcrut5/index.html` on December 29, 2020.

[6]Downloaded from Makiko Sato's webpage at `http://www.columbia.edu/~mhs119` on December 29, 2020.

The recalcitrant component is common to all locations, so that the fast component accounts for all spatial heterogeneity in temperature anomalies. Calculating the entire distribution of the fast component from the entire distribution of anomalies is accomplished by subtracting the recalcitrant component from the support of the distribution. For example, the probably mass of the anomaly at 1°C in 2000 has a recalcitrant component of $0.1 - 0.08 = 0.02$°C, so is assigned to the fast component of $1 - 0.02 = 0.98$°C. Doing so for all anomalies results in a fast component distribution in 2000 which is that of the anomalies in 2000 only shifted to the left by 0.02°C.

4.2 Main Estimation Results

4.2.1 Step 1: $df(r)/dh$.

Densities of the HadCRUT5 temperature anomalies are estimated on a compact support that excludes 1% of the outliers of the distribution of temperature anomalies across the entire time span following Chang *et al.* (2020) and Miller and Nam (2020). The support is then adjusted to also accommodate densities of the fast component as discussed above, so that the same support is used for both densities across all years. The support employed is $[-5.40, 5.58]$ with increments of $\epsilon = 0.005$, so that the sample size $n+1$ is $(r^+ - r^-)/\epsilon + 1 = 2,197$ for each year. Density estimation is accomplished using a Bartlett kernel density estimator with Silverman bandwidth.

Figure 1 compares three series: (a) the published HadCRUT5 ensemble mean GMTA, (b) GMTA using the global distributions estimated from disaggregated HadCRUT5 data, and (c) the global mean fast components calculated using the estimated fast component distributions. The figure shows that the distribution estimates yield means that align well with the published means, and that the fast component accounts for nearly all of the temperature change over the observational record, as expected. The appendix contains a detailed comparison of constructions of the published and estimated means.

Figure 2 shows estimates of the derivative $df(r)/dh$ from Step 1 for both the temperature anomaly and fast component distributions, along with 95% confidence intervals created using a first-order sieve bootstrap with 999 replications. The sieve allows for temporal correlation at specific anomalies r_i. The residuals of the sieve are drawn contemporaneously, so that any cross-sectional correlation is preserved.

The shape that these derivatives display is sensible. Any change in a density must sum to zero along its domain, because both the original density and the density that results from the change must sum to unity. A change in TRF does not seem to affect the probability of observing the most extreme positive or negative outliers in an absolute sense: they are still

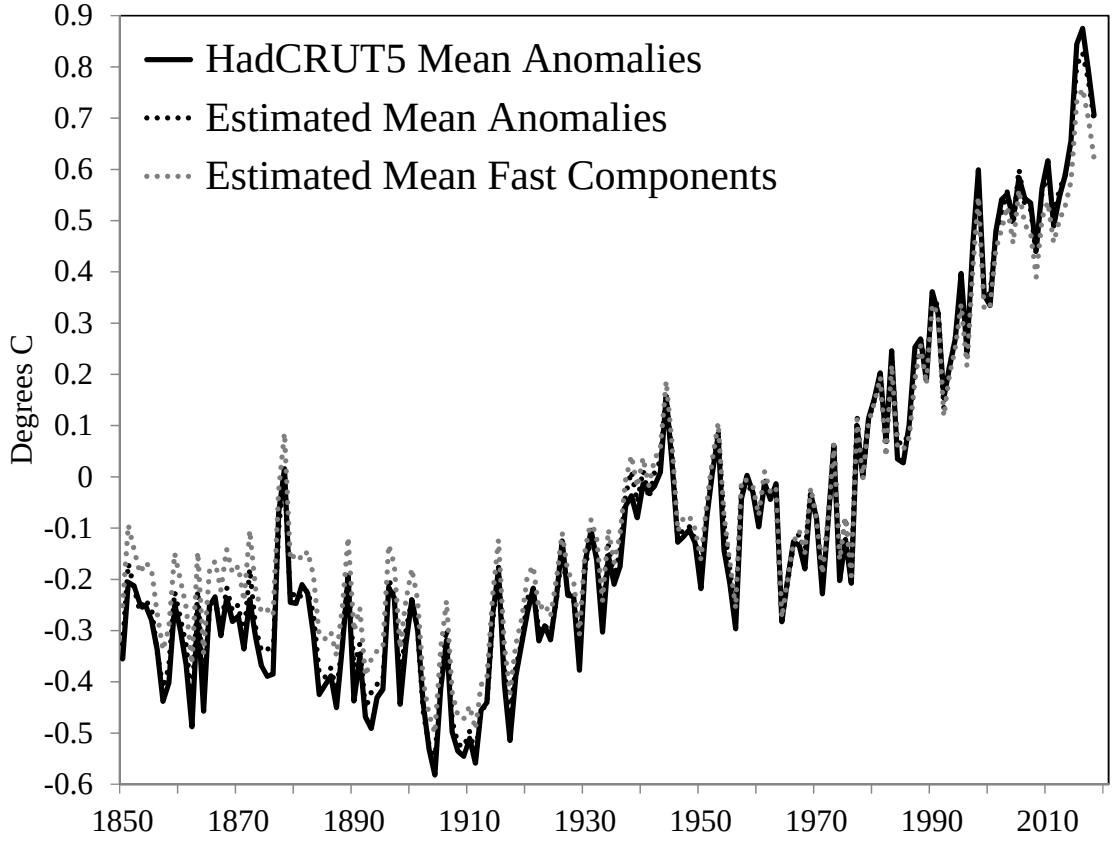

Figure 1: **HadCRUT5 and Estimated Means.** *HadCRUT5 Mean Anomalies* denotes published HadCRUT5 ensemble mean GMTA. *Estimated Mean Anomalies* ($\bar{r}_t$) denote estimates of the HadCRUT5 GMTA using the global distribution of anomalies. *Estimated Mean Fast Components* ($\bar{r}_t^F$) are analogous to Estimated Mean Anomalies but are constructed using the global distribution of fast components.

outliers with low probabilities of occurring.

Over the domain of $df(r)/dh$, the change in observing negative anomalies is mostly decreasing in TRF and the change in observing positive anomalies is entirely increasing in TRF, consistent with GMTA increasing with TRF – i.e., consistent with global warming. The set of derivatives for the fast components generally have smaller magnitudes than those of the anomalies because the fast components are less sensitive to TRF by design. This difference is not statistically significant, however.

4.2.2 Step 2: Climate Sensitivity, $1/\lambda$.

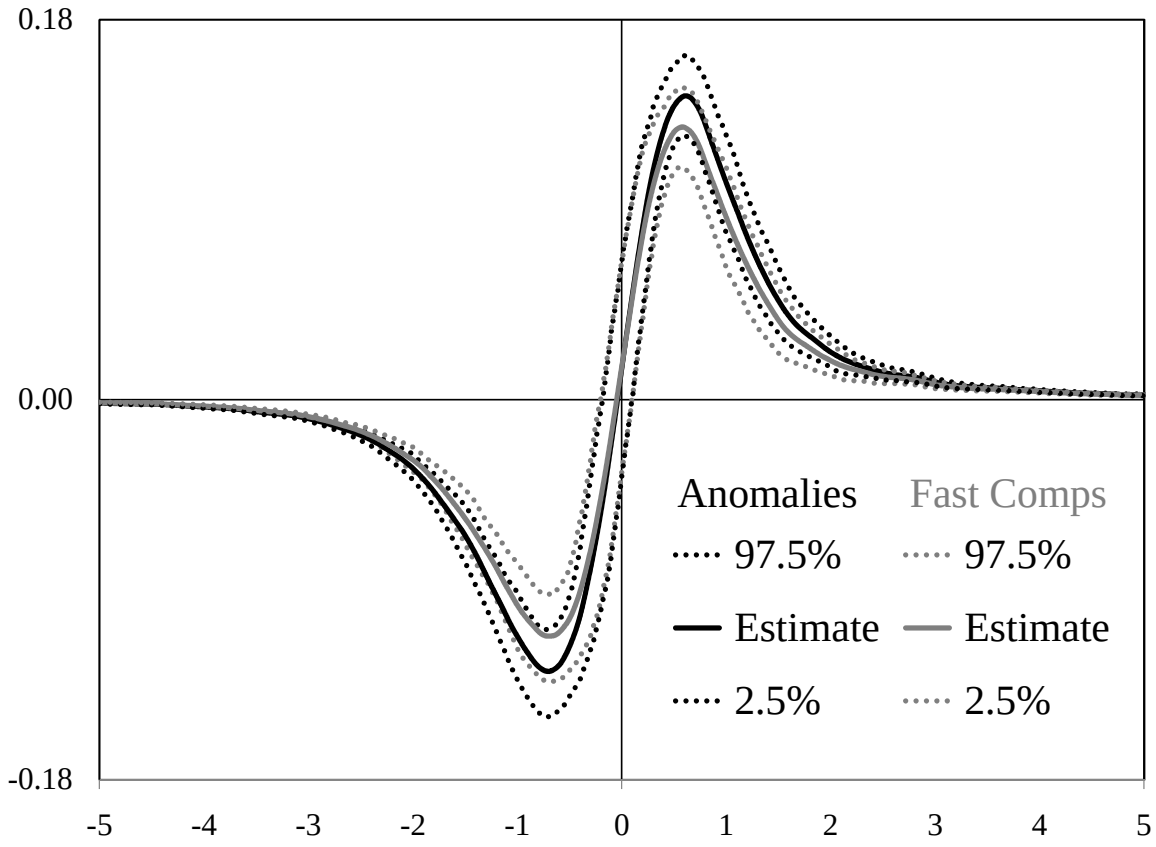

Figure 2: **Estimates of $\mathbf{df(r)/dh}$.** Estimated using temperature anomalies and their fast components, with 95% uncertainty intervals constructed using a first-order sieve bootstrap as described in the text.

Climate sensitivity estimates, or more precisely global mean climate sensitivity estimates, are shown in Table 1. The least squares estimate of α_1 from estimating Model $S0$ is given by $0.434°\text{C}/(\text{W}/\text{m}^2)$, which is comparable to those in the extant literature. For example, Estrada *et al.* (2013b) obtain $0.40°\text{C}/(\text{W}/\text{m}^2)$ using a filtered sample mean series from an earlier version of the HadCRUT data.

The TCR, given by $h_{2\times}d\bar{\tau}/dh$, is estimated to be $3.71 \times 0.434 = 1.610°\text{C}$ with an interval estimate of $(1.466, 1.750)°\text{C}$ using Model S0, well within the IPCC's "likely" range of 1-2.5°C (Bindoff *et al.*, 2013). Model $S0^+$, which is the static model including the recalcitrant component d_t, gives a global mean climate sensitivity of $0.376°\text{C}/(\text{W}/\text{m}^2)$, which is lower but still with a plausible TCR of 1.394°C.

The dynamic models allow muted responses of $0.180°\text{C}/(\text{W}/\text{m}^2)$ and $0.154°\text{C}/(\text{W}/\text{m}^2)$ after only one year, but the long-run responses, $0.448°\text{C}/(\text{W}/\text{m}^2)$ and $0.389°\text{C}/(\text{W}/\text{m}^2)$, are

Model	α_1	CS in °C/(W/m^2)	95% Conf. Int.	TCR in °C	95% Conf. Int.
$S0$	0.434	0.434	$(0.395, 0.472)$	1.610	$(1.466, 1.750)$
S^+0	0.376	0.376	$(0.336, 0.415)$	1.394	$(1.248, 1.539)$
D^-0	0.180	0.448	$(0.381, 0.528)$	1.662	$(1.413, 1.959)$
$D0$	0.154	0.389	$(0.322, 0.473)$	1.443	$(1.193, 1.754)$

Table 1: **Estimates of Climate Sensitivity $1/\lambda$ and Transient Climate Response.** Least squares estimates from models $S0$, S^+0, D^-0, and $D0$. Climate sensitivity (labeled CS) is calculated as $\alpha_1/(1-\rho)$ with $\rho = 0$ for static models, with 95% uncertainty intervals constructed using a first-order sieve bootstrap as described in the text.

quite close to those of the static models as they should be. The TCRs from the dynamic models are 1.662°C for Model D^-0 and 1.443°C for Model $D0$, quite similar to those from the corresponding static models and well within margins of error.

Notice that an increasing recalcitrant temperature component decreases the climate sensitivity and therefore the TCR, because the recalcitrant component is invariant with respect to forcings on a short time scale. The intermediate Models S^+0 and D^-0 will not be considered henceforth because there is little difference between the long-run results from Models $S0$ and D^-0 and those from Models $D0$ and S^+0.

4.2.3 Step 3: NHT Function, $X(r)$.

The flexible Fourier functional form, which approximates g by a series of polynomial and trigonometric functions, has been used to estimate semiparametric cointegrating regressions under different assumptions (Park and Hahn, 1999; Park *et al.*, 2010). This form may be written as

$$g_j^S(s) = \begin{cases} s^j & \text{for} \quad j = 2, ..., p \\ \cos 2\pi k s & \text{for} \quad j = p + 2k - 1 \quad \text{and} \quad k = 1, ..., q \\ \sin 2\pi k s & \text{for} \quad j = p + 2k \quad \text{and} \quad k = 1, ..., q \end{cases}$$

for $s \in [0, 1]$. Using this notation, $m = p + 2q$.

The functions g_j^S must be defined over the unit interval, so let $g_j(r) = (r^+ - r^-)g_j^S((r - r^-)/(r^+ - r^-))$. Thus,

$$\langle g_j(r), f_t(r) \rangle = \left\langle (r^+ - r^-)g_j^S((r - r^-)/(r^+ - r^-)), f_t(r) \right\rangle$$

holds, so that the inner products in equations (17) and (21) can be evaluated even though g_j^S is defined on the unit interval. Table 2 shows estimates of δ_1 and Δ from Models $S1$ and $D1$ in equations (17) and (21). Because the point of these regressions is orthogonalization

	Model $S1$			Model $D1$		
	$-\delta_1$	Δ		$-\delta_1$	Δ	
x_{2t}	0.295	1.000	0.000	0.203	1.000	0.000
x_{3t}	4.987	0.091	1.000	4.946	0.100	1.000

Table 2: **Estimates of $-\delta_1$ and $\boldsymbol{\Delta}$.** Least squares estimates based on the regressions implied by equations (17) and (21) with residuals denoted by x_{2t} and x_{3t}. Estimates of δ_0 and δ_{-1} are not displayed because they are not used for identification.

	Model $S1$		Model $D1$	
	est.	s.e.	est.	s.e.
ρ	–	–	0.546	0.064
α_0	−0.352	0.012	−0.132	0.021
α_1	0.440	0.013	0.180	0.026
β_2	0.104	0.031	0.065	0.029
β_3	−0.192	0.097	−0.120	0.083

Table 3: **Estimates of Models S1 and D1.** Least squares estimates based on the regressions in (18) and (20).

rather than estimation, standard errors are not reported.

Next, β in Model $S1$ in equation (18) or Model $D1$ in equation (20) is estimated using least squares. Selection of p and q may be accomplished using an information criterion, such as Bayesian (BIC) or Hannan-Quinn (HQ). Setting the maximum of (p, q) to be $(2, 2)$, or $m = 6$, BIC and HQ are minimized at $(2, 0)$ and $(1, 1)$ respectively for Model $S1$. The results presented here use the HQ choice $(1, 1)$, or $m = 3$ (no polynomial terms, a single set of periodic functions), which are qualitatively similar to those using $(2, 0)$. The specification is fixed to $(1, 1)$ in Model $D1$ for comparison with Model $S1$.

Estimates from Models $S1$ and $D1$ in equations (18) and (20) are shown in Table 3. Standard errors given in the table should be interpreted with caution, because they are not robust to nuisance parameters that may result from trending data. More robust and meaningful interval estimates are presented subsequently. Estimates of α_1 are numerically comparable to those obtained in the previous step, but these are not intended to estimate climate sensitivity. Estimates of climate sensitivity are still given by those in Table 1.

Estimates of β, δ_1, and Δ in Tables 2 and 3 are used to identify $\gamma_1 = -\beta'\delta_1$ and $\gamma'_{2:m} = \beta'\Delta$, and then $\gamma_0 = -\gamma_1 \langle \iota, f \rangle - \gamma'_{2:m} \langle g_{2:m}, f \rangle$. Finally, $\gamma_1 r + \gamma'_{2:m} g_{2:m}(r)$ is identified by multiplying $\gamma_1 s$ and $g_j^S(s)$ by $(r^+ - r^-)$ to recover r and $g_j(r)$ for $j = 2, ..., m$.

Before proceeding and in light of the multiple steps leading up to this point, it is useful to consider uncertainty in estimation of the NHT and thus the local climate sensitivity. Uncertainty in estimation of $df(r)/dh$ and $1/\lambda$ were both dealt with by way of a first-order

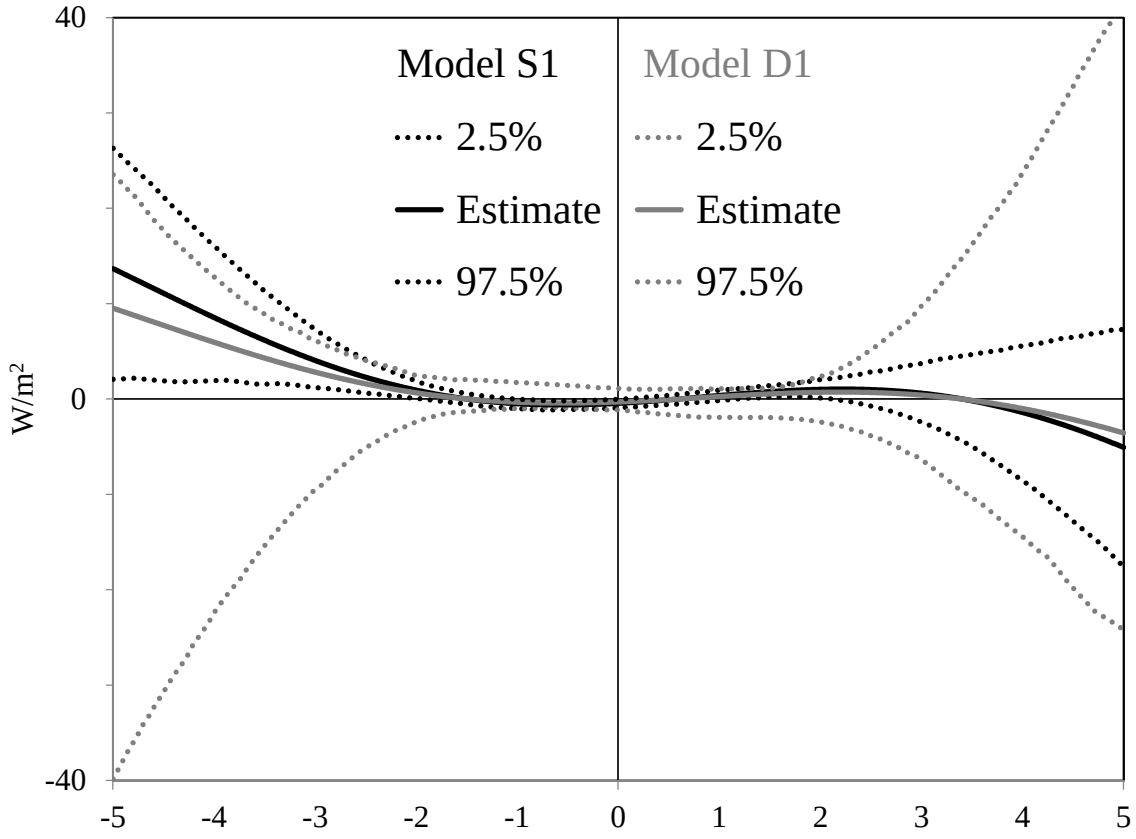

Figure 3: **Estimates of NHT $\mathbf{X}(\mathbf{r})$.** Estimated using Model $S1$ and Model $D1$, with 95% uncertainty intervals constructed using a first-order sieve bootstrap as described in the text.

sieve bootstrap with 999 replications, so it is natural to deal with uncertainty in estimating β and thus γ_0, γ_1, and $\gamma_{2:m}$ in a similar way.

The bootstrap strategy redraws the fitted residuals from equation (18) or (20). However, the terms in $x_{2:m,t}$ are not re-orthogonalized with respect to the bootstrapped regressand. An estimate of $X(r)$ also requires an estimate of $\alpha_{S0,1} = 1/\lambda$, so the respective bootstrap samples must be drawn jointly. In other words, pseudo-samples are drawn using the same random seed for $X(r)$ as for $\alpha_{S0,1}$ in the previous step.

Figure 3 shows the NHT function $X(r)$ in W/m^2. In spite of the uncertainty, $X(r)$ is clearly nonconstant and nonlinear, inconsistent with a zero-dimensional EBM (homogenous planet). However, as discussed above, the nonlinearity in r is *not* inconsistent with the one-dimensional Budyko-Sellers EBM. Because there appears to be little statistical difference between the Models $S1$ and $D1$, but the former is estimated more precisely, we henceforth focus exclusively on the results from Model $S1$.

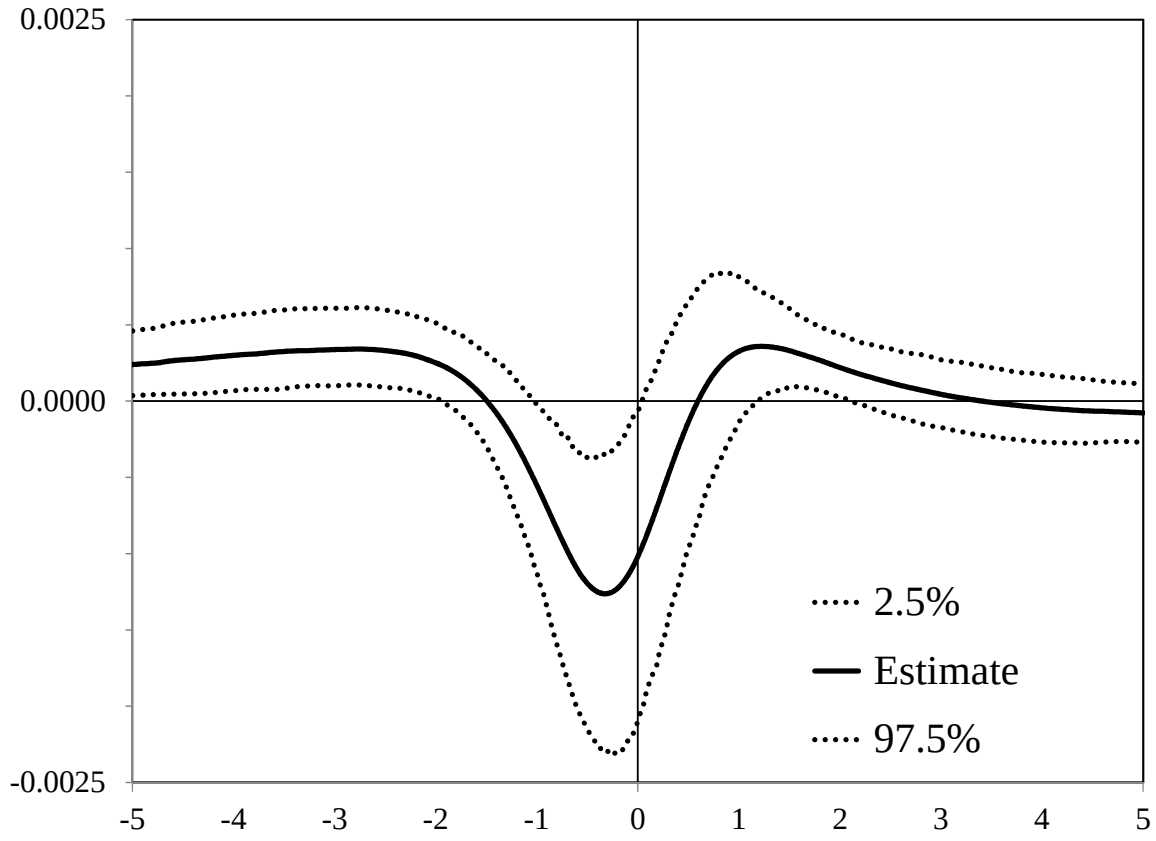

Figure 4: **Estimates of $\mathbf{X}(\mathbf{r})\mathbf{f}(\mathbf{r})$.** Estimates using Model $S1$, with 95% uncertainty interval constructed using first-order sieve bootstrap as described in the text.

The magnitudes of the point estimates of the NHT function, on the order of ± 10 W/m^2, are considerably less than those estimated in the extant literature. For example, Trenberth *et al.* (2001) estimate positive zonal averages up to 50 W/m^2 and negative zonal averages down to about -125 W/m^2. The smaller magnitudes of the present analysis are likely attributable to the aggregation of locations and months with the same temperature anomaly to create the temperature distribution for the statistical analysis.

Figure 3 is easy to interpret as the NHT function, but not as easy to read, because outlying values of the graph dominate. With this is mind, Figure 4 shows $X(r)f(r)$, which may be interpreted roughly as NHT at a given temperature anomaly weighted by the probability of observing that anomaly. Under this weighting, it is easier to see a statistically significant difference between the estimated function and a constant or otherwise linear function.

It is clear from Figure 4 that coldest anomalies correlate with positive (outgoing) NHT

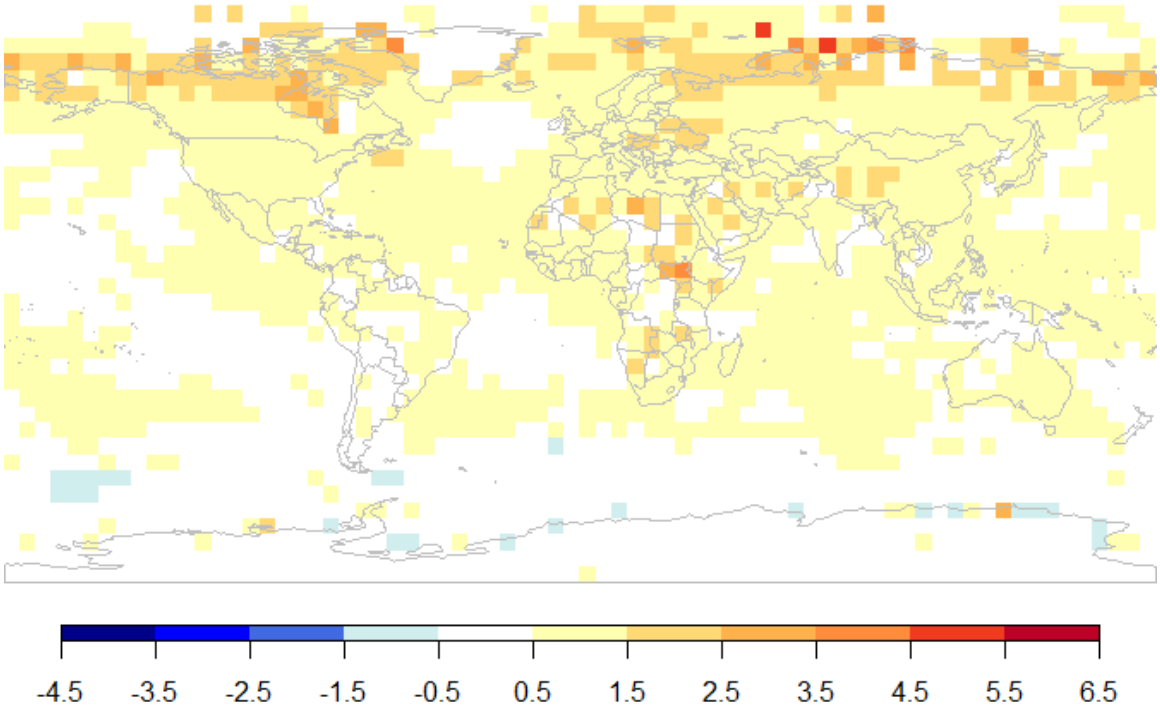

Figure 5: **Temperature Anomalies, in °C.** 10-year average over 2009-2018.

– i.e., these areas tend to export energy. In contrast, moderately negative or positive anomalies, over roughly -1.5°C to 0.6°C, correlate with negative (incoming) NHT – these areas tend to import energy. Over roughly 0.6°C to 3.0°C, NHT is positive again but no longer statistically significant beyond 2.0°C.

Figure 5 shows a map of HadCRUT5 temperature anomalies averaged over 120 months, 2009-2018. Figure 6 maps the locationless NHT function $X(r)$ in Figure 3 to locations in Figure 5 based on the average anomaly component over this period. NHT over most of the globe are estimated to be less than 1.0 W/m^2 in absolute value. That this number is quite low in comparison with those in Figure 3 above results from the averaging of the anomalies over time used to generate the figure. Very few areas have sustained anomalies of a particularly large magnitude.

Areas with positive NHT tend to be those with warmer or near-zero anomalies in Figure 5. This tendency seems counter-intuitive in light of the point estimate of the NHT function in Figure 3, which is mostly downward sloping. However, the finding results from the NHT function being negative between about -1.5°C and 0.6°C and positive between about 0.6°C and 3.0°C. There are very few observations more extreme than -1.5°C or 3.0°C. This finding may be interpreted to mean that while energy exporting areas are warming up,

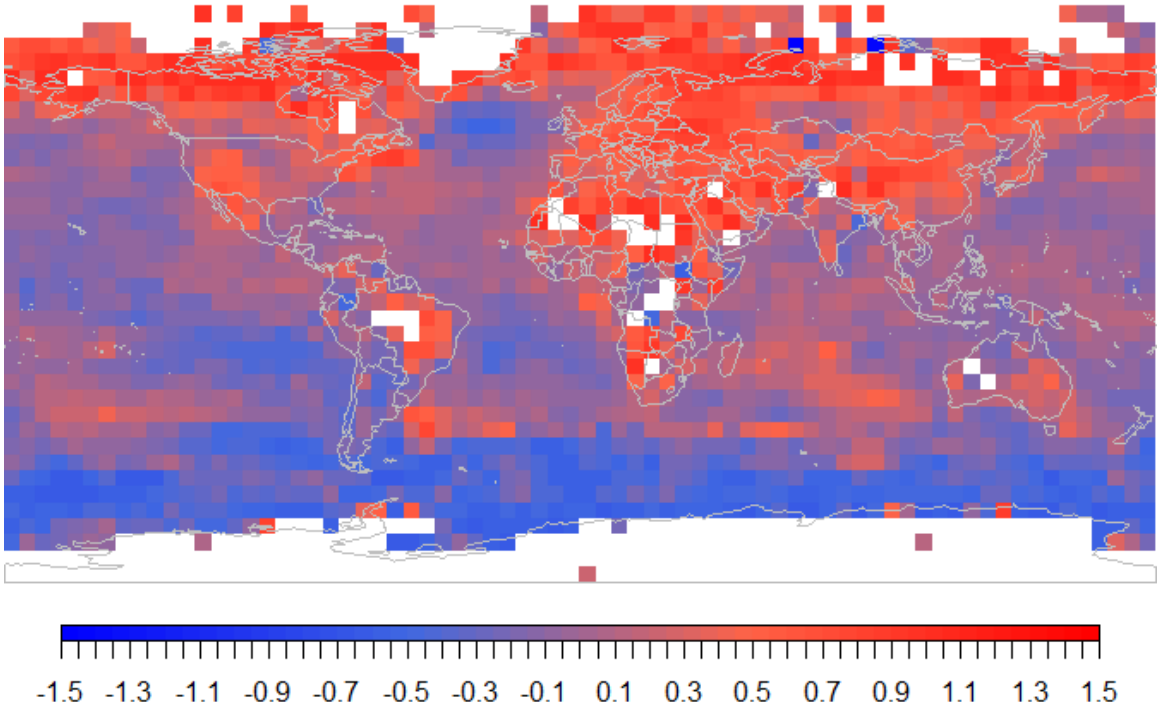

Figure 6: **Estimates of NHT X(r) from Model S1 Mapped to Location, 2009-2018, in W/m^2.** White cells denote either missing anomaly data from Figure 5 (most) or $X(r)$ estimated to be outside of $[-1.5, 1.5]$ W/m^2 (few).

energy importing areas are not warming up as fast. Such an interpretation is reasonable because the capacity of areas to export energy is bounded by their geographical features, which do not change over time. Exports cannot keep up with forcings, so areas that export energy are warming up the most.

NHT tends to be positive over continental landmasses, so that landmasses generally export energy to the oceans. Trenberth *et al.* (2001) found the net effect to be the opposite over a longer and earlier time period, citing the strength of the ocean's moderation of temperatures over land during the Northern Hemisphere winter to that during the summer. On the other hand, evidence of a divide in the Southern Hemisphere between the cold Antarctic Circumpolar Current and the warm currents of the southern gyres of the South Pacific, South Atlantic, and Indian Oceans is roughly consistent with their findings. Figure 6 does not show a similar divide in the Northern Hemisphere. Estimated NHT conforms more to the asymmetry of landmasses across the hemispheres than to symmetry in latitude imposed by traditional one-dimensional EBMs.

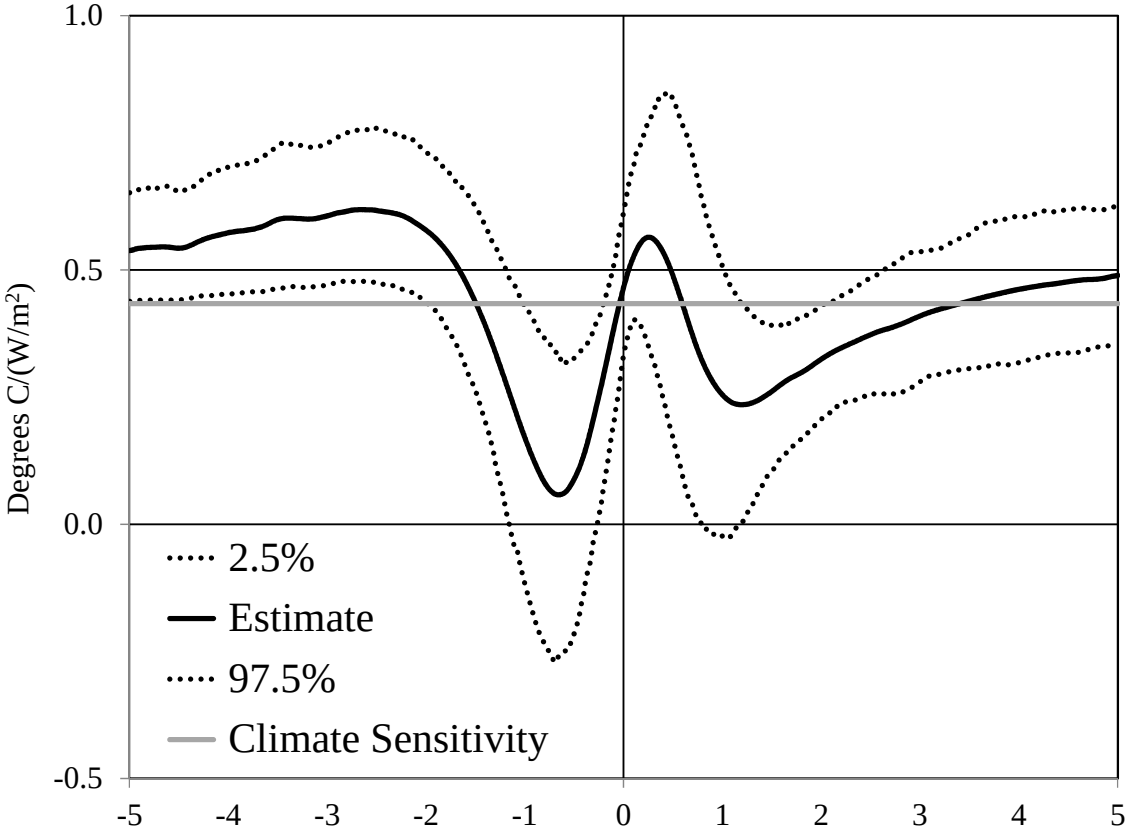

Figure 7: **Estimates of LCS $\mathbf{C(r)}$, in $\mathbf{°C/(W/m^2)}$.** Estimated using Model $S1$, with 95% uncertainty interval constructed using a first-order sieve bootstrap as described in the text. For reference, the global mean climate sensitivity estimated to be $1/\lambda = 0.434°\text{C}/(\text{W/m}^2)$ is plotted.

4.2.4 Synthesis: Local Climate Sensitivity, $C(r)$.

Finally, the steps are synthesized to estimate LCS $C(r)$. Figure 7 shows the result using Model $S1$. Results using Model $D1$ (not shown) mostly lie within the uncertainty interval for Model $S1$ but have a much wider uncertainty interval around them. The 95% confidence intervals are constructed by drawing from the same empirical error distributions resulting from first-order sieve bootstraps as discussed above, but it is important to fix the random seed, so that the bootstrapped distribution of $C(r)$ preserves correlations between the bootstrapped distributions of the individual components.

As a reference, recall that the point estimate of global mean climate sensitivity estimated in Step 2 is $0.434°\text{C}/(\text{W/m}^2)$ and the mean LCS given here is $0.440°\text{C}/(\text{W/m}^2)$. The difference $0.006°\text{C}/(\text{W/m}^2)$ is attributable to variation in $X(r)$ over time. As discussed above, a time-varying intercept may be identified, so that the last term in equation (10)

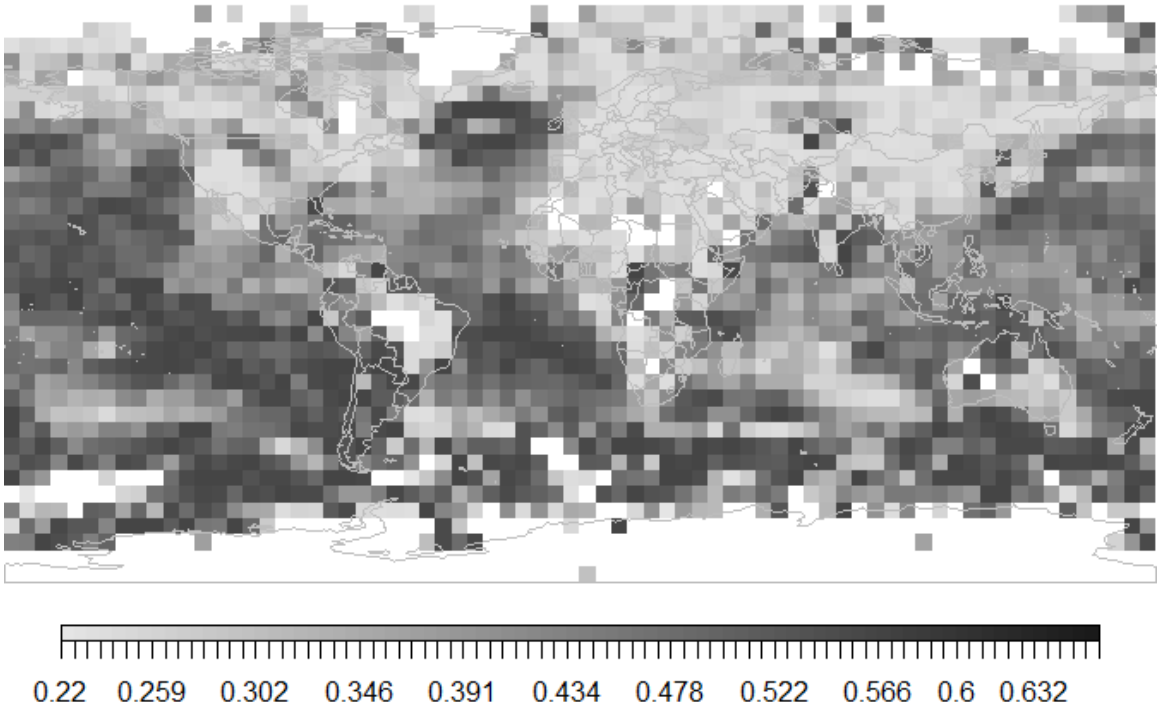

Figure 8: **Estimates of $\mathbf{C(r)}$ from Model S1 Mapped to Location, 2009-2018, in $\mathbf{^\circ C/(W/m^2)}$.** White cells denote either missing anomaly data from Figure 5 (most) or $C(r)$ estimated to be outside $[0.22, 0.66]^\circ\text{C}/(\text{W}/\text{m}^2)$ (a few smaller; none larger).

is not assumed to be zero. Because this difference is well within the margin of error of estimating climate sensitivity and does not have very much impact on the shape of the LCS, the assumption of time-invariance is plausible.

LCS exceeds the global mean climate sensitivity at particularly cold anomalies, decreasing dramatically as the temperature anomaly warms with a trough at about -0.667°C. The point estimate of the nadir exceeds $0^\circ\text{C}/(\text{W}/\text{m}^2)$, but negative LCSs are within the range of uncertainty. LCS then increases dramatically and crosses the global mean climate sensitivity at an anomaly close to zero and peaks (again) just above zero. The horizontal distance between this peak and the trough is on the order of 1°C. The LCS has one more trough and then increases to the level of the global mean again. The total range estimated by the point estimates from Model $S1$ is $0.058^\circ\text{C}/(\text{W}/\text{m}^2)$ to $0.564^\circ\text{C}/(\text{W}/\text{m}^2)$.

Similar to Figure 6, Figure 8 presents LCS geographically. Some striking patterns emerge. Areas that were light or dark red in Figure 6 tend to be light gray in Figure 8, meaning that areas with a positive energy balance – that export rather than import energy – are less sensitive to TRF. The most sensitive areas, darker gray in Figure 8, tend to be energy importers, blue in Figure 6. This relationship is consistent with the minus sign in

front of $X(r)$ in equation (11) derived from the physical model.

The difference between positive and negative NHT is especially noticeable in the ocean regions. Most are more sensitive than average, with a few large "islands"of insensitivity, particularly noticeable in the southern parts of the Indian, Pacific, and Atlantic, but also at mid-latitudes of the Western coast of Mexico and Eastern coast of Canada.

Going back to Figure 5, those areas that are the most sensitive to TRF appear to have experienced no more than a 0.5°C increase over the base period, which seems counter-intuitive. Note especially the Atlantic regions off the coasts of Greenland and Brazil. In contrast, the areas that have experienced increases of more than 0.5°C may have no more than average sensitivity. This is possible because the most sensitive areas tend to be over oceans, which are net importers of energy. Manabe *et al.* (1991), Sejas *et al.* (2014), *inter alia* attribute the disparity in temperature responses over ocean and land to ocean heat storage and especially to evaporation over the ocean, both of which ameliorate warming.

The LCS estimated here from the historical record is somewhat comparable to the negative inverse of the measure of climate sensitivity mapped by Boer and Yu (2003, Figure 3) using simulated values from an equilibrium over 500 years in the future. They obtain $1/\lambda$ roughly twice as large as the value $0.434°\text{C}/(\text{W}/\text{m}^2)$ obtained here and those used or obtained by a number of other authors. It is difficult to compare the magnitudes of their measure of local climate sensitivity with those presented here, because the inverse creates an asymptote near zero, but the signs may be compared.

Most notably, Boer and Yu (2003) also find the oceans to be relatively sensitive but with a pocket of negative sensitivity in the Central Pacific and negative values particularly to the south and around Antarctica. Sensitivities around Antarctica, given by about $-1/7 = -0.14°\text{C}/(\text{W}/\text{m}^2)$ in some localities in their analysis, are roughly comparable to the low end of the uncertainty interval of sensitivities in the present analysis that map to similar regions. Boer and Yu (2003) also find the area around the North Pole, Hudson and Baffin Bays, and Central Asia to be negatively sensitive. In the present analysis using historical data rather than simulated data, these areas have positive sensitivity though some are quite low.

5 Concluding Remarks

The statistical methodology proposed in this paper estimates local climate sensitivity, a disaggregation of climate sensitivity as defined by Boer and Yu (2003) *inter alia*, using well-known aggregated forcings and disaggregated temperature anomaly data sets over the historical record. The underlying physical model is a hybrid of existing one- and two-

dimensional energy balance models, in the sense that the data are subject to some aggregation similarly to one-dimensional EBMs, but that variation within latitudes is allowed similarly to two-dimensional EBMs.

Both static and dynamic statistical models are proposed and estimated, with some specifications that also allow for the decomposition of temperatures into recalcitrant and fast components, along the lines of Held *et al.* (2010) and Bindoff *et al.* (2013). However, as those authors note, the recalcitrant component does not contribute substantively over the historical record, so our main results are based on models that do not distinguish between these components. The methodology is semiparametric but each step employs techniques no more complicated than least squares or kernel density estimation.

Estimates of local horizontal NHT are intermediate to those of the LCS estimates. The estimated NHT function is strongly nonconstant and nonlinear in temperature anomalies, which is not inconsistent with the linear one-dimensional Budyko-Sellers EBM, because temperature anomalies rather than levels are used.

Areas of the globe with estimated positive NHT tend to be those with warmer anomalies. These areas also tend to be over land, suggesting that landmasses are net exporters of energy to oceans. Some similarities emerge with NHT mapped in the extant literature (Trenberth *et al.*, 2001), especially in the Southern Hemisphere.

In turn, local climate sensitivity is estimated with a global mean climate sensitivity of $0.434°\text{C}/(\text{W}/\text{m}^2)$ which is consistent with the extant literature (Estrada *et al.*, 2013b). The total range over the globe is estimated to be $0.058°\text{C}/(\text{W}/\text{m}^2)$ to $0.564°\text{C}/(\text{W}/\text{m}^2)$, but mostly above about $0.22°\text{C}/(\text{W}/\text{m}^2)$. The smaller values are roughly comparable to those of Boer and Yu (2003), as are the regions over which the sensitivity is very low or possibly negative.

The heterogeneity of local climate sensitivity detected and estimated here has broad economic implications. Polar amplification allowed by such heterogeneity drives more severe weather at mid-latitudes (Francis and Vavrus, 2012; Liu *et al.*, 2012; IPCC, 2014), implying an increase in economic damages in addition to the rising mean predicted by zero-dimensional EBMs. Furthermore, Brock and Xepapadeas (2017) emphasize the differences in economic costs of climate change and bias in mitigation policies from ignoring heterogeneity in NHT.

Future research linking local climate sensitivity to local damage functions, such as those used by Miller and Brock (2021) based on those of Gasparrini *et al.* (2015) for relative risk of mortality or those of Hsiang *et al.* (2017) for a number of climate-induced damages, may further scientific knowledge about the heterogeneity and economic disparity expected from climate change.

Appendix

A.1 A Discrete Representation of the EBM

Hemispheric mean temperature in a model that varies only over latitude is defined as

$$\bar{\tau} = \int_0^{\pi/2} \tau_\theta \cos\theta d\theta$$

(cf. Held and Suarez, 1974), where the cosine adjusts for the curvature of the Earth. For temperature that also varies over longitude, the global average is

$$\bar{\tau} = \frac{1}{4\pi} \int_{-\pi}^{\pi} \int_{-\pi/2}^{\pi/2} \tau_{\theta\varphi} \cos\theta d\theta d\varphi,$$

with the convention that τ_{00} is the temperature where the Prime Meridian intersects the Equator. Division by 2π converts longitude from radians and division by 2 averages the hemispheric means evaluated over positive and negative latitudes.

Generalizing the one-dimensional EBM in equation (4) to vary over longitude yields

$$X_\tau(\tau_{\theta\varphi} - \bar{\tau}, \theta, \varphi) = h + QS(\theta) - A - \lambda\tau_{\theta\varphi}, \tag{22}$$

where the subscript τ denotes that the function X is defined with respect to the temperature rather than its anomaly. S reflects mean annual radiation (North *et al.*, 1981), so it varies over latitude but not over longitude.

However, global observational data sets report temperature anomalies relative to a base period in order to ameliorate known measurement errors and biases in the data. Although the temperature τ is effectively observable at a single location (θ, φ) where a temperature reading is taken, the base temperature relies on aggregation of many observations and thus is not generally observable at a single location, especially over oceans where observations rely on ships. Instead, the set of all locations on the surface of the globe is divided into n disjoint subsets ("boxes") such that the union of all n of these subsets covers the surface of the globe. In particular, these sets are created by a grid with intervals of equal latitude and equal longitude. For mathematical convenience, no boxes overlap the Equator and locations on the borderline between multiple boxes are assigned systematically to only one box.

Let $L(\theta, \varphi)$, or simply box L, denote the subset that contains (θ, φ). For a generic

function $G(\tau_{\theta\varphi}, \theta, \varphi)$ define

$$G(\tau_L, L) = \frac{1}{2\pi} \iint\limits_L w_L(\theta) G(\tau_{\theta\varphi}, \theta, \varphi) d\theta d\varphi,$$

where the double integral aggregates the function over the box with weights

$$w_L(\theta) = \cos\theta \left(\frac{1}{2\pi} \iint\limits_L \cos\theta d\theta d\varphi \right)^{-1}$$

given by the cosine of latitude divided by the total surface area of the box.

In particular, the expression

$$\tau_L = \frac{1}{2\pi} \iint\limits_L w_L(\theta) \tau_{\theta\varphi} d\theta d\varphi,$$

gives the mean temperature for box L. Moreover, the expression

$$X_\tau(\tau_L, L) = \frac{1}{2\pi} \iint\limits_L w_L(\theta) X_\tau(\tau_{\theta\varphi} - \bar{\tau}, \theta, \varphi) d\theta d\varphi$$

gives the NHT function for box L. And, finally, the expression

$$S(L) = \frac{1}{2\pi} \iint\limits_L w_L(\theta) S(\theta) d\theta d\varphi$$

gives the mean annual radiation for box L.

The base temperature is defined by averaging τ_L over a base period. We denote the base temperature by τ_L^B and treat it as fixed over time. The temperature anomaly for box L is thus defined by $r_L = \tau_L - \tau_L^B$ using the observed values of τ_L and τ_L^B for each box. Finally, defining a function X such that

$$X(r_L, L) = X_\tau((r_L - \bar{r}) - (\tau_L^B - \bar{\tau}^B), L) = X_\tau(\tau_L, L),$$

where $\bar{r} = \bar{\tau} - \bar{\tau}^B$ is the GMTA and $\bar{\tau}^B$ is the mean of temperatures across the globe during the base period, and integrating equation (22) over the box yields the two-dimensional EBM given by equation (5) in Section 2.

A.2 Approximations to the EBM

Suppose that the range over which observed surface anomalies vary is given by $[r^-, r^+]$, and define disjoint subsets $L(r) = \{L : r_L = r\}$ of the set of all locations such that the union of all of these locations over $[r^-, r^+]$ covers the surface of the globe. In particular, $L(r)$ is the set of all boxes in which the temperature anomaly takes a value of r. For a generic function $G(\tau_L, L)$ define

$$G(r) = \int\limits_{L(r)} w_{L(r)}(\theta) G(\tau_L, L) dL,$$

where

$$w_{L(r)}(\theta) = \cos\theta \left(\frac{1}{2\pi} \iint\limits_{L(r)} \cos\theta d\theta d\varphi \right)^{-1}$$

is defined similarly to w_L above, but weights for the surface area of all boxes for which an anomaly r is observed rather than that of a single box.

An approximation used by Chang *et al.* (2020) and Miller and Nam (2020) and employed in the present analysis is to treat each of the boxes as being equally sized – i.e., $G(\tau_L, L) \approx G(\tau_L)$ is assumed. Along these lines, define

$$\bar{G}(r) = \int\limits_{L(r)} \bar{w}_{L(r)} G(\tau_L) dL$$

with

$$\bar{w}_{L(r)} = \left(\frac{1}{2\pi} \iint\limits_{L(r)} d\theta d\varphi \right)^{-1}$$

or, equivalently, define

$$\bar{G}(r) = n_r^{-1} \sum_{L(r)} G(r_L)$$

with n_r defined to be the number of anomalies in the set $L(r)$.

We may define $X(r)$ from $X(r_L, L)$ using either $G(r)$ or $\bar{G}(r)$ and $S(r)$ analogously from $S(\theta)$ to obtain equation (6) from equation (5). In practice, we estimate equation (6) using the equal-sized box approximation to facilitate the interpretation of the distribution function $f(r)$ as a spatial distribution.

A.3 Estimators of GMTA

There are multiple ways to approximate GMTA. The simplest,

$$\bar{r} \approx n^{-1} \sum_{L} r_L,$$

simply weights all anomalies equally as $\bar{G}(r)$ does. A more sophisticated method weights the anomalies by the surface area of the boxes as $G(r)$ does. Yet another method estimates GMTA by

$$\int_{r^-}^{r^+} r\hat{f}(r)dr \approx \int_{r^-}^{r^+} r \left(\frac{1}{2\pi} \iint_{L(r)} \bar{w}_{L(r)} f(r) d\theta d\varphi \right) dr$$

by defining $\hat{f}(r)$ to be an estimate of the density $f(r)$ of anomalies at each box.

The first and third methods both assign equal weights to each box, but they differ in that the first estimates the population mean with the sample mean, while the third estimate the population mean using an estimate of the population density. The second uses a sample mean like the first but weights boxes by their surface area. Figure 1 shows that the latter two – the most dissimilar of the three – are in fact quite similar, suggesting the adequacy of approximation by equal weighting.

References

Bindoff, N.L., P.A. Stott, K.M. AchutaRao, M.R. Allen, N. Gillett, D. Gutzler, K. Hansingo, G. Hegerl, Y. Hu, S. Jain, I.I. Mokhov, J. Overland, J. Perlwitz, R. Sebbari and X. Zhang, 2013, Detection and attribution of climate change: From global to regional, in: Stocker, T.F., D. Qin, G.-K. Plattner, M. Tignor, S.K. Allen, J. Boschung, A. Nauels, Y. Xia, V. Bex and P.M. Midgley, (Eds.), Climate change 2013: The physical science basis. Contribution of working group I to the Fifth Assessment Report of the Intergovernmental Panel on Climate Change. Cambridge University Press, Cambridge, pp. 867-952.

Boer, G.J and B. Yu, 2003, Climate sensitivity and response, Climate Dynamics 20, 415-429.

Brock, W.A. and A. Xepapadeas, 2017, Climate change policy under polar amplification, European Economic Review 94, 263-282.

Bruns, S.B., Z. Csereklyei, and D.I. Stern, 2000, A multicointegration model of global

climate change, Journal of Econometrics 214, 175-197.

Budyko, M.I., 1969, The effect of solar radiation variations on the climate of the Earth, Tellus 21, 611-619.

Castruccio, S., D.J. McInerney, M.L. Stein, F.L. Crouch, R.L. Jacob, and E.J. Moyer, 2014, Statistical emulation of climate model projections based on precomputed GCM runs, Journal of Climate 27, 1829-1844.

Chang, Y., Y. Choi, C.S. Kim, J.I. Miller, and J.Y. Park, 2016a, Disentangling temporal patterns in elasticities: A functional coefficient panel analysis of electricity demand, Energy Economics 60, 232-243.

Chang, Y., R.K. Kaufmann, C.S. Kim, J.I. Miller, J.Y. Park, and S. Park, 2020, Evaluating trends in time series of distributions: A spatial fingerprint of human effects on climate, Journal of Econometrics 214, 274-294.

Chang, Y., C.S. Kim, J.I. Miller, J.Y. Park, and S. Park, 2014, Time-varying long-run income and output elasticities of electricity demand, Energy Economics 46, 334-347.

Chang, Y., C.S. Kim, J.I. Miller, J.Y. Park, and S. Park, 2016b, A new approach to modeling the effects of temperature fluctuations on monthly electricity demand, Energy Economics 60, 206-216.

Chang, Y., C.S. Kim, and J.Y. Park, 2016c, Nonstationarity in time series of state densities, Journal of Econometrics 192, 152-167.

Chapman, S.C., D.A. Stainforth, and N.W. Watkins, 2013, On estimating local long-term climate trends, Philosophical Transactions of the Royal Society A 371, 20120287.

Eroğlu, B.A., J.I. Miller, and T. Yiğit, 2022, Time-varying cointegration and the Kalman filter, Econometric Reviews 41, 1-21.

Estrada, F. and P. Perron, 2014, Detection and attribution of climate change through econometric methods, Boletín de la Sociedad Matemática Mexicana 20, 107-136.

Estrada, F., P. Perron, C. Gay-García, and B. Martínez-López, 2013a, A time-series analysis of the 20th century climate simulations produced for the IPCC's fourth assessment report, PLoS ONE 8, e60017.

Estrada, F., P. Perron, and B. Martínez-López, 2013b, Statistically derived contributions of diverse human influences to twentieth-century temperature changes, Nature Geoscience 6, 1050-1055.

Francis, J.A. and S.J. Vavrus, 2012, Evidence linking Arctic amplification to extreme weather in mid-latitudes, Geophysical Research Letters 39, L06801.

Gasparrini A., Y. Guo, M. Hashizume, E. Lavigne, A. Zanobetti, J. Schwartz, A. Tobias, S. Tong, J. Rocklöv, B. Forsberg, M. Leone, M. De Sario, M.L. Bell, Y.-L.L. Guo, C. Wu, H. Kan, S.-M. Yi, M. de S.Z.S. Coelho, P.H.N Saldiva, Y. Honda, H. Kim, and B. Armstrong, 2015, Mortality risk attributable to high and low ambient temperature: A multicountry observational study, The Lancet 386, 369-375.

Gregory, J.M. and P.M. Forster, 2008, Transient climate response estimated from radiative forcing and observed temperature change, Journal of Geophysical Research 113, D23105.

Hansen, J., M. Sato, P. Kharecha, K. von Schuckmann, D.J. Beerling, J. Cao, S. Marcott, V. Masson-Delmotte, M.J. Prather, E.J. Rohling, J. Shakun, P. Smith, A. Lacis, G. Russell, and R. Ruedy, 2017, Young people's burden: requirement of negative CO2 emissions, Earth System Dynamics 8, 577-616.

Held, I.M. and M.J. Suarez, 1974, Simple albedo feedback models of the icecaps, Tellus 26, 613-629.

Held, I.M., M. Winton, K. Takahashi, T. Delworth, F. Zeng, and G.K. Vallis, 2010. Probing the fast and slow components of global warming by returning abruptly to preindustrial forcing, Journal of Climate 23, 2418-2427.

Hsiang, S., R. Kopp, A. Jina, J. Rising, M. Delgado, S. Mohan, D.J. Rasmussen, R. Muir-Wood, P. Wilson, M. Oppenheimer, K. Larsen, and T. Houser, 2017, Estimating economic damage from climate change in the United States, Science 356, 1362-1369.

IPCC, 2014, Climate change 2014: Synthesis report. Contribution of working groups I, II and III to the Fifth Assessment Report of the Intergovernmental Panel on Climate Change [Core Writing Team, R.K. Pachauri and L.A. Meyer (eds.)]. IPCC, Geneva.

Kaufmann, R.K., H. Kauppi, M.L. Mann, and J.H. Stock, 2013, Does temperature contain a stochastic trend: Linking statistical results to physical mechanisms, Climatic Change 118, 729-743.

Kaufmann, R.K., H. Kauppi, and J.H. Stock, 2006a, Emissions, concentrations and temperature: A time series analysis, Climatic Change 77, 249-278.

Kaufmann, R.K., H. Kauppi, and J.H. Stock, 2006b, The relationship between radiative forcing and temperature: What do statistical analyses of the instrumental temperature record measure? Climatic Change 77, 279-289.

Kaufmann, R.K., H. Kauppi, and J.H. Stock, 2010, Does temperature contain a stochastic trend? Evaluating conflicting statistical results, Climatic Change 101, 395-405.

Kaufmann, R.K. and D.I. Stern, 2002, Cointegration analysis of hemispheric temperature relations, Journal of Geophysical Research 107, 4012.

Langen, P.L. and V.I. Alexeev, 2007. Polar amplification as a preferred response in an idealized aquaplanet GCM, Climate Dynamics 29, 305-317.

Leduc, M., H.D. Matthews, and R. de Elía, 2016, Regional estimates of the transient climate response to cumulative CO2 emissions, Nature Climate Change 6, 474-478.

Liu, J., J.A. Curry, H. Wang, M. Song, and R.M. Horton, 2012, Impact of declining Arctic sea ice on winter snowfall, Proceedings of the National Academy of Sciences of the United States of America 109, 4074-4079.

Manabe S., R.J. Stouffer, M.J. Spelman, and K. Bryan, 1991, Transient responses of a coupled ocean-atmosphere model to gradual changes of atmospheric CO2. Part I: Annual mean response, Journal of Climate 4, 785-818.

Merlis, T.M. and M. Henry, 2018, Simple estimates of polar amplification in moist diffusive energy balance models, Journal of Climate 31, 5811-5824.

Miller, J.I. and W.A. Brock, 2021, Beyond RCP8.5: Marginal mitigation using quasi-representative concentration pathways, Journal of Econometrics, forthcoming.

Miller, J.I. and K. Nam, 2020, Dating hiatuses: a statistical model of the recent slowdown in global warming and the next one, Earth System Dynamics 11, 1123-1132.

Morice, C. P., J.J. Kennedy, N.A. Rayner, J.P. Winn, E. Hogan, R.E. Killick, R.J.H. Dunn, T.J. Osborn, P.D. Jones, and I.R. Simpson, 2020, An updated assessment of near-surface temperature change from 1850: the HadCRUT5 dataset, Journal of Geophysical Research, in press.

Nam, K., 2018, Essays on climate econometrics, PhD dissertation, University of Missouri.

North, G.R., 1975, Theory of energy-balance climate models, Journal of Atmospheric Sciences 32, 2033-2043.

North, G.R., R.F. Cahalan, and J.A. Coakley, Jr., 1981, Energy balance climate models, Reviews of Geophysics and Space Physics 19, 91-121.

North, G.R., J.G. Mengel, and D.A. Short, 1983, Simple energy balance model resolving the seasons and the continents: Application to the astronomical theory of the ice ages, Journal of Geophysical Research 88, 6576-6586.

Pagan, A., 1984, Econometric issues in the analysis of regressions with generated regressors, International Economic Review 25, 221-247.

Park, J.Y. and S.B. Hahn, 1999, Cointegrating regressions with time varying coefficients, Econometric Theory 15, 664-703.

Park, J.Y. and J. Qian, 2012, Functional regression of continuous state distributions, Journal of Econometrics 167, 397-412.

Park, J.Y., K. Shin, and Y.J. Whang, 2010, A semiparametric cointegrating regression: Investigating the effects of age distributions on consumption and saving, Journal of Econometrics 157, 165-178.

Peixoto, J.P. and A.H. Oort, 1992, Physics of climate, American Institute of Physics, New York.

Pretis, F., 2020, Econometric models of climate systems: The equivalence of energy balance models and cointegrated vector autoregressions, Journal of Econometrics 214, 256-273.

Schwartz, S.E., 2012, Determination of Earth's transient and equilibrium climate sensitivities from observations over the twentieth century: Strong dependence on assumed forcing, Surveys in Geophysics 33, 745-777.

Screen, J.A. and I. Simmonds, 2013, Exploring links between Arctic amplification and mid-latitude weather, Geophysical Research Letters 40, 959-964.

Sejas, S.A., O.S. Albert, M. Cai and Y. Deng, 2014, Feedback attribution of the land-sea warming contrast in a global warming simulation of the NCAR CCSM4, Environmental Research Letters 9, 124005.

South, A., 2011, rworldmap: A new R package for mapping global data, The R Journal 3, 35-43.

Sellers, W.D., 1969, A global climatic model based on the energy balance of the earth-atmosphere system, Journal of Applied Meteorology 8, 392-400.

Sellers, W.D., 1976, A two-dimensional global climatic model, Monthly Weather Review 104, 233-248.

Siler, N., G.H. Roe, and K.C. Armour, 2018, Insights into the zonal-mean response of the hydrologic cycle to global warming from a diffusive energy balance model, Journal of Climate 31, 7481-7493.

Stern, D.I. and R.K. Kaufmann, 2000, Detecting a global warming signal in hemispheric temperature series: A structural time series analysis, Climatic Change 47, 411-438.

Taylor, F.W., 2005, Elementary Climate Physics, Oxford University Press, Oxford.

Trenberth, K.E., J.M. Caron, and D.P. Stepaniak, 2001, The atmospheric energy budget and implications for surface fluxes and ocean heat transports, Climate Dynamics 17, 259-276.